Robust differentiation of human enteroendocrine cells from intestinal stem cells

Daniel Zeve[1,2], Eric Stas[1,†], Joshua de Sousa Casal[3,†], Prabhath Mannam[1], Wanshu Qi[1], Xiaolei Yin[4,5,#], Sarah Dubois[1,6], Manasvi S. Shah[1,2], Erin P. Syverson[2,3], Sophie Hafner[1], Jeffrey M. Karp[5,7,8], Diana L. Carlone[1,2,8], Jose Ordovas-Montanes[3,7], David T. Breault[1,2,8,*]

[1]Division of Endocrinology, Boston Children's Hospital, Boston, MA 02115, USA

[2]Department of Pediatrics, Harvard Medical School, Boston, MA 02115, USA

[3]Division of Gastroenterology, Boston Children's Hospital, Boston, MA 02115, USA

[4]David H. Koch Institute for Integrative Cancer Research, Massachusetts Institute of Technology, Cambridge, MA 02139, USA

[5]Center for Nanomedicine and Division of Engineering in Medicine, Department of Medicine, Brigham and Women's Hospital, Harvard Medical School, Harvard-MIT Division of Health Sciences and Technology, Boston, MA 02115, USA

[6]School of Arts and Sciences, MCPHS University, Boston, MA 02115, USA

[7]Broad Institute of MIT and Harvard, Cambridge, MA 02142, USA

[8]Harvard Stem Cell Institute, 7 Divinity Avenue, Cambridge, MA 02138, USA

[†]Authors contributed equally to this work

[*]Corresponding author

[#]Current address: Institute for Regenerative Medicine, Shanghai East Hospital, Frontier Science Center for Stem Cell Research, School of Life Sciences and Technology, Tongji University, Shanghai, China

ABSTRACT

Enteroendocrine (EE) cells are the most abundant hormone-producing cells in humans and are critical regulators of energy homeostasis and gastrointestinal function. Challenges in converting human intestinal stem cells (ISCs) into functional EE cells, *ex vivo*, have limited progress in elucidating their role in disease pathogenesis and in harnessing their therapeutic potential. To address this, we employed small molecule targeting of key transcriptional regulators, GATA4, JNK and FOXO1, known to mediate endodermal development and hormone production, together with directed differentiation of human ISCs from the duodenum and rectum. We observed marked induction of EE cell differentiation and gut-derived expression and secretion of SST, 5HT, GIP, CCK, GLP-1 and PYY upon treatment with various combinations of three small molecules: rimonabant, SP600125 and AS1842856. Robust differentiation strategies capable of driving human EE cell differentiation is a critical step towards understanding these essential cells and the development of cell-based therapeutics.

INTRODUCTION

Enteroendocrine (EE) cells are found throughout the gastrointestinal (GI) tract and represent the most abundant hormone-producing cell type within mammals. EE cells, as a whole, secrete a large variety of hormones, including glucose-dependent insulinotropic polypeptide (GIP), cholecystokinin (CCK), serotonin (5HT), somatostatin (SST), peptide YY (PYY), and glucagon-like peptide-1 (GLP-1), among others[1,2]. In response to physiological and nutritional cues, EE cells, through the production of these various hormones, are responsible for regulating multiple aspects of GI activity and nutritional homeostasis[1,2]. Because of this, EE cells have been implicated in the pathogenesis of GI diseases such as irritable bowel syndrome and inflammatory bowel disease, as well as metabolic diseases such as type 2 diabetes mellitus[3-5].

52 Similar to other mature intestinal epithelial cells, EE cells are derived from ISCs, which reside
53 within the crypts of Lieberkuhn[6]. In recent years, much progress has been made understanding
54 the mechanisms underlying ISC self-renewal and differentiation using 3D-organoid culture[7-10].
55 Using combinations of growth factors and small molecules targeting specific transcriptional
56 regulators and signaling pathways, intestinal organoids can either be maintained predominantly
57 as ISCs or differentiated into mature intestinal cells of either the absorptive or secretory
58 lineages[11,12]. For example, maintenance of ISC self-renewal requires activation of canonical Wnt
59 signaling using WNT3a and R-spondin, suppression of bone morphogenic protein (BMP)
60 signaling using Noggin, and inhibition of p38 MAPK signaling using the small molecule
61 SB202190[9-11]. By altering these pathways along with transcriptional regulators, strategies have
62 begun to emerge to direct ISC differentiation into mature intestinal epithelial cell types[8,9,13].
63
64 EE cells are defined by expression of the specific hormone each produces and their location
65 along the GI tract[2,14-16]. These cells also express multiple neuroendocrine secretory proteins,
66 including Chromogranin A (CHGA), some of which are more specific to certain EE cell types
67 than others[14,15]. Further, multiple transcription factors are critical for EE cell differentiation and
68 function, including neurogenin 3 (NEUROG3), neuronal differentiation 1 (NEUROD1), and
69 paired box 4 (PAX4)[1,2,10]. Pancreatic and duodenal homeobox 1 (PDX1) has also been shown to
70 regulate gene expression in a subpopulation of EE cells located within the duodenum[17]. The
71 directed differentiation of human EE cells requires the removal of Wnt ligands and inhibition of
72 Notch signaling but, in contrast to mice, human EE cells do not differentiate in the presence of
73 p38 MAPK inhibitors[9,10,16]. Through the use of an inducible NEUROG3 system, multiple studies
74 have shown induction of the human EE cell lineage, with expression and secretion of multiple
75 hormones in organoid cultures of both the small and large intestine[14,18-21]. However, while strong
76 mRNA expression of multiple mature EE markers has been observed, limited data exist showing

77 robust protein expression of EE cell markers using small molecule differentiation
78 protocols[8,9,16,22,23].
79
80 Additional factors and signaling pathways have also been implicated in EE cell formation and
81 function. For example, GATA Binding Protein 4 (GATA4) plays a role in small intestine formation
82 and an important role in the expression of CCK and GIP, as GATA4 has been shown to bind to
83 the GIP promoter[24] and *Gata4* deletion in mice leads to reduced expression of both GIP and
84 CCK[25-28]. C-Jun N-terminal Kinase (JNK) signaling, which has been implicated in regulating
85 ISCs[29,30], also regulates beta cell function through its actions on PDX1[31,32], and has been
86 suggested to upregulate EE cell differentiation, with deletion of JNK2 reducing the number of
87 CHGA-positive (CHGA+) cells in mouse organoids[33]. The role of JNK in the regulation of EE cell
88 differentiation and PDX1 expression has not been studied in directed differentiation of human
89 ISCs. Inhibition of Forkhead box protein O1 (FOXO1), a transcription factor critical for stem cell
90 function and energy homeostasis[34,35], has been associated with upregulation of multiple
91 endocrine-associated transcription factors and hormones, including NEUROG3 and GIP[36-38]. In
92 human intestinal organoids (HIOs) derived from induced pluripotent stem cells, transduction of a
93 dominant negative FOXO1 yielded increased numbers of CHGA+ cells, less 5HT-positive cells,
94 and no change in GLP-1 or SST-positive cells when compared to control organoids at 230
95 days[39]. Further, it has been suggested that endocannabinoid signaling, through the cannabinoid
96 receptor type 1 (CB1), inhibits CCK secretion[40], while BMP4 has been shown to induce the
97 expression of various EE hormones in human intestinal organoids[16]. However, aside from
98 BMP4, how the above factors and pathways impact directed differentiation of EE cells has been
99 largely unstudied.
100
101 Here, we establish robust EE cell differentiation protocols for human duodenal organoids
102 (enteroids) and rectal organoids (rectoids) using various combinations of small molecules

103 (rimonabant, SP600125 and AS1842856) suggested to alter the activity of GATA4, JNK, and
104 FOXO1, respectively. In enteroids, treatment with rimonabant (Rim) and SP600125 (SP) leads
105 to marked induction of *CHGA* expression and a corresponding increase in the number of
106 CHGA+ cells, as well as in the expression of multiple hormones, including SST, 5HT, CCK, and
107 GIP. Separately, treatment with AS1842856 (AS) also induced SST, 5HT, and GIP, with an
108 even stronger induction of CHGA+ cells. Comparing levels of hormone secretion, AS leads to a
109 greater induction of 5HT secretion, but less GIP, whereas the combination of Rim and SP (RSP)
110 leads to a greater induction of GIP secretion, but less 5HT. The combination of AS treatment
111 followed by RSP leads to even higher expression of *SST*, and increased secretion of GIP and
112 5HT, when compared to RSP treatment alone. In rectoids, treatment with base differentiation
113 media (DM) alone induces an increase in the number of CHGA+ cells, as well as increased
114 expression, production and secretion of GLP-1 and PYY, EE hormones predominantly produced
115 in the distal GI tract[2]. Together, these robust EE cell differentiation protocols, employing only
116 small molecules, provide important new insights into human EE cell differentiation, with
117 potentially important implications for understanding disease pathogenesis and development of
118 cell-based therapeutics.
119

120 **RESULTS**

121 **Differentiation Media Induces *CHGA* Expression in Human Duodenal Enteroids**

122 To optimize human EE cell differentiation, we developed a DM (Supplementary Table 1) by
123 combining specific components from published protocols used to induce EE cells[9,12,16,23],
124 including Wnt3a and two additional small molecules associated with endocrine cell
125 differentiation: (1) betacellulin, a ligand of both EGFR and the ErbB4 receptors[41,42] and (2)
126 PF06260933 (PF), a small molecule inhibitor of MAP4K4[43]. Human enteroids were first cultured
127 in growth media (GM, Supplementary Table 1) for two days, allowing for ISC expansion,
128 followed by DM for 12 days (G2D12). Enteroids maintained for 14 days in GM (G14) were used

129 as controls to assess for changes in gene expression. In contrast to previous strategies aimed
130 at generating EE cells over a five-day period[9,16], exposure to DM for 12 days was compatible
131 with maintenance of enteroid structural integrity (Fig 1a), possibly due to the continued
132 presence of WNT3a.
133
134 To quantify the effectiveness of DM to induce EE cell differentiation, we profiled the gene
135 expression of *CHGA* and other lineage markers, including atonal BHLH transcription factor 1
136 (*ATOH1*, secretory progenitor cells), mucin 2 (*MUC2*, goblet cells), lysozyme (*LYZ*, Paneth
137 cells), intestinal alkaline phosphatase (*ALPI*, enterocytes) and leucine-rich repeat-containing G-
138 protein coupled receptor 5 (*LGR5*, ISCs). In addition, we assessed the expression of
139 transcription factors required for duodenal EE differentiation and function (*PDX1, PAX4,*
140 *NEUROG3*, and *NEUROD1*), as well as hormones secreted from the duodenum (*CCK*, *SST*,
141 and *GIP*). To allow for relative comparison to native tissue expression levels, total RNA from
142 whole duodenal mucosal biopsies was included in each qPCR analysis. Exposure of enteroids
143 to G2D12 induced consistent expression of *CHGA*, *PAX4*, *SST*, and *GIP*, with significantly
144 higher levels of *ALPI* and significantly lower expression of *LGR5* when compared to G14 (Fig 1b
145 and Supplementary Fig 1a). Despite G2D12's ability to induce EE and enterocyte markers when
146 compared to G14, their overall expression levels remained considerably lower than whole
147 duodenal mucosa. Levels of *PDX1*, *NEUROD1*, *NEUROG3*, *CCK*, *ATOH1*, and *LYZ* were
148 unchanged compared to G14, with *MUC2* showing a trend towards higher expression in G2D12
149 enteroids (Fig 1b and Supplementary Fig 1a). Finally, despite induction in *CHGA* mRNA levels
150 in response to G2D12, analysis of CHGA protein using immunofluorescence staining and flow
151 cytometric analysis revealed fewer than 0.1% of all cells to be CHGA+, showing a trend towards
152 higher expression compared to G14 (Fig 1b-1e).
153

154 Removal of WNT3a has been shown to aid EE differentiation[9,10,16]. Analysis of enteroids
155 cultured in DM without WNT3a (G2D12-Wnt) revealed undetectable expression levels of *CHGA*
156 and *SST*, reduced *MUC2* expression, and increased *ALPI* expression when compared with
157 enteroids differentiated with WNT3a (G2D12+Wnt) (Fig 1f). To determine whether *CHGA*
158 expression was increased at an earlier time-point during the 14-day differentiation protocol, we
159 performed time-course studies and found that *CHGA* expression was undetectable in enteroids
160 cultured in G2D12-Wnt, while those exposed to G2D12+Wnt showed expression after six days
161 of starting DM (Supplementary Fig 1b). Furthermore, two of the three enteroid lines exposed to
162 G2D12-Wnt showed low total RNA levels around the eighth day of differentiation, consistent
163 with failure to maintain these lines (Supplementary Fig 1c). Therefore, we concluded that the
164 presence of WNT3a in DM is necessary to sustain enteroids in long-term culture (14 days) and
165 is not detrimental to EE differentiation. We also evaluated the impact of including betacellulin
166 and PF in our DM and found that both factors led to increased expression of EE cell markers
167 compared with GM and DM without betacellulin or PF, as well as maintaining *ALPI* levels when
168 compared to DM (Supplementary Fig 1d and 1e). Together, these data indicate that our
169 differentiation protocol markedly induced expression of some EE cell marker genes (e.g., *CHGA*
170 and *PAX4*), but is not sufficient to induce a significant increase in the number of CHGA+ EE
171 cells compared to undifferentiated controls.
172

173 **Treatment with Rimonabant and SP600125 Induces Duodenal EE Lineage Differentiation**

174 To identify additional strategies that might further induce EE cell differentiation, we focused on
175 small molecules shown to target GATA4 and PDX1 activity, key transcriptional regulators
176 involved in gastrointestinal development and hormone regulation. First, we utilized Rim, a highly
177 selective cannabinoid receptor type I (CB1) inverse agonist that has been shown to increase
178 human serum GIP levels[44] and that is structurally identical to Compound 7, a molecule
179 previously shown to increase GATA4-NKX2-5 transcriptional activity *in vitro*[45]. In parallel, we

180 used the small molecule SP to inhibit JNK signaling, which has been shown to suppress PDX1
181 activity[31,32].
182
183 Separately, both Rim and SP induced expression of multiple EE lineage markers (*CHGA,*
184 *NEUROG3, SST*, and *GIP*) when added to DM, with Rim having a much larger effect
185 (Supplementary Fig 2a). Together, RSP yielded even further increases in *SST* and *GIP*
186 expression compared to Rim or SP alone. Both PDX1 and GATA4 expression were unchanged
187 under all experimental conditions (Supplementary Fig 2a). Based on these results, Rim and SP
188 were used in combination for all subsequent experiments. The addition of RSP to DM
189 maintained overall enteroid structural integrity during the 14-day differentiation protocol (Fig 2a
190 and Supplementary Fig 2b). Moreover, compared to enteroids grown in G14 and G2D12,
191 treatment with RSP led to the upregulation of multiple EE markers (*CHGA*, *PAX4*, *NEUROD1*,
192 *NEUROG3*, *CCK*, *SST*, and *GIP*) to levels approximating whole duodenal mucosa (Fig 2b).
193 Other lineage markers were also increased with RSP exposure, including *ATOH1*, *MUC2*, *LYZ*,
194 *ALPI*, and *LGR5* when compared to G14 and *ATOH1*, *MUC2*, and *LGR5* when compared to
195 G2D12 (Supplementary Fig 2c). Immunofluorescence staining for CHGA showed multiple
196 positive cells within individual enteroids (Fig 2c), with a large majority of enteroids (83%)
197 containing CHGA+ cells (Fig 2d). By comparison, only 1.0% of enteroids grown in G2D12 were
198 CHGA+ (Fig 2d). Quantitative flow cytometric analysis revealed 1.4% of all cells treated with
199 RSP were CHGA+, almost seven times the number seen with G2D12 alone (Fig 2e).
200
201 **Treatment with AS1842856 Induces Duodenal EE Lineage Differentiation**
202 Next, we assessed the impact of adding AS, a well-described FOXO1 inhibitor[46], to our
203 differentiation protocol. Addition of AS led to the formation of small, spherical enteroids (Fig 3a
204 and Supplementary Fig 3a). Compared to enteroids grown in G14 and G2D12, AS treatment led
205 to the upregulation of multiple EE markers (*CHGA*, *PAX4*, *PDX1*, *NEUROD1*, *NEUROG3*, *SST,*

206 and *GIP*), many to levels approximating whole duodenal mucosa. The only exception to this was
207 *CCK*, which was significantly lower in AS when compared to G14 (Fig 3b). In addition, AS
208 increased expression of other secretory and ISC markers, including *ATOH1*, *MUC2*, and *LGR5*,
209 when compared to G14 and G2D12 (Supplementary Fig 3b). Interestingly, the use of AS
210 reduced expression of the enterocyte marker *ALPI* when compared to G14 and G2D12,
211 suggesting a possible role for FOXO1 inhibition in the induction of the secretory lineage
212 (Supplementary Fig 3b). Immunofluorescence staining revealed CHGA+ cells within a large
213 majority of individual enteroids (85%) (Fig 3c and 3d). By comparison, only 3% of enteroids
214 grown in G2D12 had CHGA+ cells (Fig 3d). Quantitative flow cytometric analysis revealed 5.2%
215 of all cells exposed to AS to be CHGA+, almost 50 times the number seen with G2D12 alone
216 (Fig 3e).
217
218 **Treatment with Rimonabant/SP600125 or AS1842856 Promote Distinct Enteroid**
219 **Differentiation Trajectories**
220 To better assess the transcriptomic distinctions between cells from the various culture
221 conditions, we utilized single cell RNA sequencing (scRNA-seq) on the 10X platform combined
222 with sample hashing, allowing us to assess the reproducibility of our findings from distinct
223 donors**.** Enteroids from three individuals were grown in G2D12, RSP or AS, for a total of nine
224 samples. After the 14-day protocol, enteroids were isolated and processed into a single-cell
225 suspension and their condition and patient source were marked using Hashtag antibodies prior
226 to pooling the samples together[47]. After labeling, cells were processed, and single-cell
227 transcriptomes were generated.
228
229 By using hashtag labeling, we were able to categorize cells into singlets (significant detection of
230 one antibody), doublets (significant detection of more than one antibody) or negative droplets
231 (no significant detection of any antibodies). Negative droplets were found to have a reduced

232 number of both detected genes and unique genes or unique molecular identifiers (UMIs),
233 supporting the idea that the majority of these datapoints do not correspond to an individual cell
234 (Supplementary Fig 4a). In contrast, both singlets and doublets had appreciable numbers of
235 both genes and UMIs detected. In addition, we found that they had similar UMIs, percentage of
236 mitochondrial RNA, which aids in identification of low-quality cells, and detected gene
237 distributions (Supplementary Fig 4a). However, upon dimensional reduction, we found that
238 singlets and doublets formed distinct groupings in both t-distributed stochastic neighbor
239 embedding (tSNE) visualization (Supplementary Fig 4b), as well as uniform manifold
240 approximation and projection (UMAP) visualization and clustering (Supplementary Figs 4b and
241 4c), indicating that although they had similar RNA content, singlets likely correspond to true
242 singlets, whereas doublets correspond to multiple cell types analyzed together in a single
243 droplet.
244
245 After removal of doublets, negative droplets, and low-quality cells (gene count < 200,
246 percentage of mitochondrial RNA > 25%), the resulting dataset consisted of 14,767 cells spread
247 across the three different culture conditions. UMAP visualization revealed distinct cell separation
248 between G2D12 and AS treatment with minimal overlap between the two populations (Fig 4a).
249 In contrast, enteroid treatment with RSP generated populations that overlapped with the two
250 other culture conditions (Fig 4a). To further characterize the developing populations within each
251 treatment, we performed Louvain clustering and identified 15 clusters within the combined
252 dataset (Supplementary Fig 4d). Of these 15 clusters, some were composed of cells sourced
253 from all three culture conditions, such as clusters 2, 4, 9, and 7, whereas other clusters were
254 primarily formed by cells from one treatment group, such as cluster 8 (AS) and cluster 3
255 (G2D12). To assist with manual annotation of each cluster, we calculated the top markers of
256 each Louvain cluster (Supplementary Fig 4e; Wilcoxon rank sum test, $p_{adj}<1.38x10^{-21}$ for
257 displayed markers)[48]. By using these markers, as well as classical markers of various epithelial

258 populations[49,50], we broadly classified the data into six populations of epithelial cells, including
259 stem cells, proliferating progenitor cells, progenitor cells, enterocytes, goblet cells and
260 enteroendocrine cells (Fig 4b). ISCs were identified by expression of *LGR5, AXIN2* and
261 *ASCL2*[51]. Enterocytes were identified by the expression of *KRT20*, *FABP2*, and *FABP1*, goblet
262 cells by the expression of *MUC2, FCGBP,* and *GFI1*, and EE cells by expression of *CHGA*,
263 *NEUROG3*, *NEUROD1*, and *PAX4*[52,53] (Fig 4c). Finally, progenitor cells were identified as
264 having a mixture of stem cell markers, albeit at a lower level than the ISCs, while also
265 expressing mature enterocyte markers. We were able to distinguish proliferating cycling
266 progenitors from other progenitor cells by expression of the proliferation marker *MKI67*[54] (Fig 4b
267 and 4c); however, some progenitor markers were also lowly expressed in secretory cell
268 populations, suggesting that these groups likely also contain secretory progenitors.
269
270 To understand how different culture conditions impacted enteroid development and
271 differentiation, we first compared the proportions of the various cell types across each condition
272 (Fig 4d). We found that treatment with G2D12 primarily gave rise to cells of the absorptive
273 lineage, with 58% identified as enterocytes. The remaining cells exposed to G2D12 consisted of
274 stem cells (5.7%), proliferating progenitor cells (5.4%) and progenitor cells (30%). G2D12 did
275 not give rise to secretory cells, with almost no detection of goblet cells (0.6%) or EE cells
276 (0.2%). In contrast to G2D12, treatment with either RSP or AS led to a decrease in the
277 proportion of enterocytes (RSP: 17%, AS: 2.5%) and an increase in stem cells (RSP: 22%, AS:
278 42%), goblet cells (RSP: 4.6%, AS: 1.5%), and EE cells (RSP: 4.3%, AS: 18%), with significant
279 differences noted between G2D12 and AS conditions for stem cells, enterocytes, and EE cells.
280
281 To further characterize the differentiation path of each culture condition, we used scVelo to
282 model the RNA velocity and differentiation trajectory of each cell type[55]. Briefly, RNA velocity
283 analysis pipelines, such as scVelo, leverage the fact that scRNA-seq can distinguish between

284 un-spliced and spliced variants of each gene. Since recently transcribed RNA is present as an
285 un-spliced variant which is then spliced into its mature form before eventually being degraded, it
286 is possible to calculate the dynamic kinetics of each individual gene's expression across all cells
287 within the dataset based on the ratio of un-spliced to spliced RNA[55,56]. scVelo uses the
288 collection of gene kinetics to infer the direction and speed of cell state changes on a population
289 level. We applied this method to each culture condition and generated vector estimates of
290 cellular transition overlaid on each UMAP (Fig 4e). In all three conditions, the majority of vector
291 arrows initiate from a stem cell cluster in the lower half of the UMAP. In the G2D12 culture
292 condition, cells primarily move towards proliferating progenitors and progenitor cells, before
293 moving towards the enterocyte cluster. In contrast, in AS treated cells, the vector arrows
294 proceed through a completely different trajectory, with the majority of vectors moving towards
295 the goblet cell cluster and then into the EE cluster. Cells treated with RSP revealed vector
296 arrows in patterns that resembled both G2D12 and AS treated cells, suggesting it may promote
297 early differentiation of both secretory and absorptive cell types. Finally, a small proportion of
298 vector arrows suggested a "backwards" trajectory, with movement from a differentiated
299 enterocyte into a progenitor population. This behavior may be indicative of de-differentiation or
300 possibly movement towards cell death, as the cells lose features associated with mature cell
301 types[57,58]. Overall, these results indicate that all three culture conditions have distinct
302 differentiation potentials, with AS and RSP giving rise to an increased proportion of EE cells
303 compared to G2D12.
304
305 Finally, to verify that the EE cells identified in our enteroid system resemble those found *in situ*,
306 we compared our dataset with a reference gene set from isolated mouse EE cells[49]. This list
307 encompasses 77 genes, including conventional markers such as *CHGA*, *NEUROG3* and the
308 enzyme *TPH1* (Supplementary Fig 4f). An EE cell gene module score was calculated for each
309 cell in our scRNA dataset based on the number of shared features with the reference EE gene

310 set[49], which revealed exclusive marking of cells within our EE cell cluster (Fig 4f). In addition,
311 when looking across culture conditions, RSP and AS showed an increased effect size in relation
312 to G2D12, with AS having a larger effect size than RSP (Fig 4g). These results underscore
313 differences observed between the three culture conditions described in previous results and
314 further demonstrate that EE cells generated using these protocols resemble those found within
315 native tissue.
316
317 **Treatment with AS1842856 Followed by Rimonabant and SP600215 Increases GIP**
318 **Expression in Human Duodenal Enteroids**
319 Compared to RSP treated enteroids, AS treatment led to more robust EE differentiation, based
320 on overall induction of multiple EE cell markers and the larger fraction of CHGA+ cells (Figs 2-
321 4). Direct comparison of the two protocols revealed that AS exposure led to higher expression of
322 *CHGA, NEUROD1*, *NEUROG3*, and *SST* (Supplementary Fig 5a), consistent with the higher
323 percentage of CHGA+ cells (Figs 2 and 3). In contrast, we noted that RSP induced higher
324 expression of *GIP* compared to AS (Supplementary Fig 5a). Given these results, we next
325 hypothesized that the combination of Rim, AS, and SP (RASP) would further increase
326 expression of both CHGA and GIP. Exposure of enteroids to RASP for the full duration of the
327 differentiation protocol, however, was not compatible with viable enteroids, as evidenced by
328 their irregular morphology and extremely low RNA content (Supplementary Fig 5b and 5c).
329
330 We next tested the impact of adding RSP after exposure to AS, reasoning that AS treatment
331 would shunt a larger proportion of cells into the EE lineage, as indicated by the scRNA-seq data
332 (Figs 4d and 4g), with the later addition of RSP inducing *GIP* expression in more cells than RSP
333 alone. To identify the appropriate time for the addition of RSP, we performed a time-course
334 analysis of AS treated enteroids and found that multiple transcription factors required for EE
335 differentiation, including *NEUROD1* and *NEUROG3*, showed increased expression around the

336 fourth day of differentiation. Following this, both *CHGA* and *SST* had detectable transcript levels
337 by the sixth day of differentiation (Supplementary Fig 6a). Given these data, we next
338 hypothesized that AS treatment for six days followed by subsequent exposure to RSP would
339 lead to increased *GIP* expression compared to RSP alone. To test this, we utilized two
340 differentiation strategies: (1) switching from AS to RSP at day six of differentiation (AS→RSP) or
341 (2) adding RSP to AS at day six of differentiation (AS→RASP). Morphologically, AS→RASP
342 produced smaller enteroids compared to other conditions (Supplementary Fig 6b); however,
343 RNA concentrations were consistently above the minimum threshold of 10 ng/μL, suggesting
344 improved viability over exposure to RASP for the full duration of the differentiation protocol
345 (Supplementary Fig 6c). Enteroids treated with AS→RSP showed gene expression changes
346 that were similar to RSP alone, aside from *CHGA* and *SST* (Fig 5a). Enteroids treated with
347 AS→RASP showed 2-3-fold higher gene expression levels of most EE cell markers when
348 compared to AS, with the exception of *PDX1* and *CCK* (Fig 5a).
349
350 Furthermore, exposure to AS for the entire differentiation protocol, i.e., AS and AS→RASP,
351 decreased expression of *MUC2* and *ALPI* and increased expression of *LGR5* compared to
352 those that received RSP alone, for any amount of time (Supplementary Fig 7a). In terms of
353 other lineages, immunofluorescence staining showed that the enterocyte marker cytokeratin 20
354 (CK20) was expressed in all differentiation conditions, but with very little stain noted in
355 AS→RASP (Supplementary Fig 7b). MUC2 staining was only noted in RSP, AS and AS→RSP
356 enteroids while LYZ, similar to CK20, was present in all differentiation conditions except
357 AS→RASP (Supplementary Fig 7c and 7d).
358
359 We also evaluated the effect of our differentiation protocols on proliferation and apoptosis after
360 7 and 14 days of culture. As expected, at 7days GM supported cell proliferation, as evidenced

361 by a significantly higher fraction of EdU-positive (EdU+) cells (2.7%) after a two-hour pulse,
362 compared to all other conditions. There were no significant differences between DM, RSP and
363 AS, which ranged from 0.1-0.5% EdU+ cells. At day 14 of culture, no differences in the
364 percentage of EdU+ cells were detected between any groups (which ranged from 0.1-0.6%),
365 suggesting that GM conditions are not able to sustain ongoing proliferation indefinitely
366 (Supplementary Fig 7e). Analysis of apoptosis at 7 days showed GM had the lowest percentage
367 of Annexin V-positive cells (13%) compared to each differentiation condition, with RSP showing
368 the highest fraction at 29%. At day 14, despite modest differences between groups, levels of
369 apoptosis were fairly consistent ranging from 19-29% (Supplementary Fig 7f). Further, enteroids
370 exposed to RSP (including RSP, AS→RSP, and AS→RASP) appear to have more apoptotic
371 cells compared to DM and AS.
372
373 All four differentiation strategies induced a high fraction of CHGA+ enteroids, ranging from 79 to
374 88% (RSP, 79%; AS, 82%; AS→RSP, 81%; AS→RASP, 88%), as assessed by immunostaining
375 (Fig 5b and 5c). Quantitative flow cytometric analysis revealed 3.7% of all cells exposed to
376 AS→RSP to be CHGA+, which was between the 1.0% seen in RSP alone and the 6.1% seen in
377 AS alone. AS→RASP had the highest percentage of CHGA+ cells at 7.1%, more than 100 times
378 the number seen with G2D12 alone (Fig 5d). Taken together, these data reveal that exposure of
379 human enteroids to AS→RASP is the most effective way to induce EE cell differentiation, in
380 terms of expression of *CHGA*, *PAX4*, *NEUROD1*, and *NEUROG3*, as well as overall number of
381 CHGA+ cells.
382
383 **Hormone Production and Secretion Mirror Gene Expression Changes in Duodenal**
384 **Enteroids**

385 To assess hormone production and secretion during EE cell differentiation, we next assayed for
386 duodenal-associated hormones in response to the various differentiation conditions.
387 Immunofluorescence staining showed that SST was expressed similarly in all differentiation
388 conditions, aside from G2D12, with 42 to 53% of enteroids containing SST-positive cells (RSP,
389 45%; AS, 42%; AS→RSP, 53%; AS→RASP, 51%) (Fig 6a and 6b). 5HT was expressed in a
390 higher percentage of enteroids treated with AS throughout the entire differentiation period than
391 those that only received RSP (RSP, 44%; AS, 75%; AS→RSP, 59%; AS→RASP, 76%) (Fig 6c
392 and 6d). An induction in GIP-positive enteroids was detected in response to all differentiation
393 conditions, with the exceptions of G2D12 and AS→RASP (RSP, 66%; AS, 53%; AS→RSP,
394 56%; AS→RASP, 8.6%) (Fig 6e and 6f). Further, CCK-positive enteroids were predominantly
395 detected in response to RSP (29%) and AS→RSP (30%) compared to all other treatment
396 groups (AS, 4.5%; AS→RASP, 2.6%) (Fig 6g and 6h).
397
398 Finally, to assess hormone secretion, we assayed conditioned media from each differentiation
399 condition. Exposure to AS alone induced higher levels of 5HT secretion than all other
400 conditions, with AS→RSP conditioned media showing higher levels of 5HT when compared to
401 RSP and AS→RASP (Fig 7a). These patterns persisted when controlled for total DNA content,
402 with the exception of a modest difference between AS→RSP and AS→RASP (Supplementary
403 Fig 8a). Importantly, secretion of 5-HT was significantly increased when differentiated enteroids
404 were exposed to the adenylate cyclase activator forskolin (Fsk) (Fig 7b and Supplementary Fig
405 8b). Secretion of GIP was highest following exposure to AS→RSP, compared to RSP alone,
406 while AS and AS→RASP treated enteroids revealed no secretion of GIP (Fig 7c and
407 Supplementary Fig 8c). Secretion of GIP from enteroids exposed to AS→RSP was also
408 significantly increased after exposure to Fsk (Fig 7d and Supplementary Fig 8d). Overall, these
409 data show that RSP and AS, either alone or in combination, can induce protein expression and

410 secretion of multiple duodenal hormones (5HT, GIP, SST and CCK) from human enteroids, with
411 specific differences depending on exposure and/or timing of RSP and AS treatment.
412
413 **Differentiation Media Induces EE Cell Differentiation in Human Rectoids**
414 To evaluate the ability of our DM to induce EE cell differentiation outside of the duodenum, we
415 exposed organoids derived from rectal ISCs (rectoids) to the G14 and G2D12 protocols
416 (Supplementary Table 1). Rectoids treated with G14 maintained spherical structures, while
417 those exposed to G2D12 had a mixture of spherical and budding structures (Fig 8a). In contrast
418 to enteroids, rectoids exposed to G2D12 had significantly increased expression of the majority
419 of EE markers, included *CHGA*, *PAX4*, *NEUROD1*, *NEUROG3*, *SST*, *GCG* and *PYY*, many of
420 which were at or above the expression level observed in whole rectal mucosa (Fig 8b). Notably,
421 rectoids exposed to G2D12 also had significantly higher expression of *ATOH1* and *MUC2*,
422 decreased expression of *LGR5*, and no change in *CAII* expression, a marker for absorptive cells
423 of the rectum[59,60], when compared to G14 (Supplementary Fig 9a).
424
425 Immunofluorescence staining revealed CHGA+ cells within a majority of G2D12 rectoids (72%)
426 (Fig 8c and 8d) and quantitative flow cytometric analysis revealed 4.7% of all cells exposed to
427 G2D12 to be CHGA+ (Fig 8e). Additional immunofluorescence staining revealed that both GLP-
428 1 and PYY were expressed in a large number of G2D12 rectoids (GLP-1, 61%; PYY, 40%) (Fig
429 8f-8i). We next assayed conditioned media from G14 and G2D12 rectoids to evaluate for
430 hormone secretion and found significant levels of both GLP-1 and PYY in G2D12 rectoids
431 compared to G14, which was increased by stimulation with Fsk (Fig 8j-8m, Supplementary Fig
432 9b-9e). Overall, these data indicate that G2D12 is sufficient to induce EE cell differentiation of
433 rectal ISCs.
434
435 **DISCUSSION**

436 Here, we establish that the addition of the small molecules rimonabant, SP600125 and
437 AS1842856 leads to robust differentiation of human EE cells from duodenal ISCs without the
438 use of transgenic modification. Prior to this, the differentiation of EE cells using only small
439 molecules had mainly been studied in the context of Wnt, Notch, MAPK and BMP signaling, with
440 inhibition of these pathways driving GI stem cells into the secretory lineage, and subsequent
441 removal of p38 MAPK inhibition leading to EE cell differentiation[8,9,16,22,23]. Despite these
442 important advances, the overall efficiency of EE differentiation in the majority of these studies is
443 hard to estimate due to their strong reliance on gene expression analysis with little data at the
444 protein level, aside from one study[22]. In this study, we show robust induction of EE
445 differentiation, assessed using gene and protein expression as well as hormone secretion, at
446 levels that approach the native duodenal mucosa.
447
448 Many of the studies establishing a role for Wnt, Notch, MAPK, and BMP signaling in EE lineage
449 differentiation have been performed using the organoid culturing system, which approximates *in*
450 *vivo* growth and development due to its 3D nature. However, there are significant shortcomings
451 to the analyses of intestinal organoid differentiation that our study has begun to address. First,
452 RNA expression does not always mirror protein expression, as evidenced by the presence of
453 *GIP* mRNA in AS→RASP enteroids (Fig 5a) with little protein expression noted on
454 immunofluorescence (Fig 6e and 6f) and no secreted protein seen on ELISA (Fig 7c). Further,
455 our study suggests that enteroids grown in G14 are not appropriate as the sole reference point
456 in differentiation experiments. For example, G2D12, but not G14, treatment induced expression
457 of *CHGA* mRNA (Fig 1b), but the comparison of enteroid mRNA expression levels to whole
458 duodenal mucosa revealed that G2D12 alone induces a very low level of *CHGA* compared to
459 native tissue. Moreover, immunodetection of CHGA expression revealed significant
460 heterogeneity between individual enteroids, even when cultured under the same experimental
461 conditions, as evidenced by only a small minority of enteroids and cells staining CHGA+ in

462 G2D12 and the variability in hormone expression using immunofluorescence seen in the other
463 differentiation conditions. These results highlight the limitations of current human EE
464 differentiation protocols.
465
466 Multiple human EE differentiation protocols using only small molecules have suggested that
467 removal of WNT3a from the base growth medium is critical for secretory lineage
468 differentiation[9,16]. Our results, in contrast, reveal that removal of WNT3a is detrimental to both
469 EE differentiation and long-term viability, as noted by a lack of *CHGA* expression at any time
470 during the differentiation protocol and a marked decrease in total RNA levels with time. This is
471 consistent with a previous study suggesting that maintaining high WNT3a concentrations during
472 differentiation was similar, if not better, at inducing *CHGA* expression than a reduction of
473 WNT3a[23]; however, that study only examined differentiation markers after two days of
474 differentiation. The currently described protocol allows for differentiation over 12 days, much
475 longer than previously published methods utilizing only small molecules[16,23]. Even though the
476 use of different reagents and source materials could be possible explanations, our data indicate
477 that removal of WNT3a is not necessary for human EE cell differentiation.
478
479 We also show that treatment of human enteroids with rimonabant, an inverse agonist of CB1
480 receptor signaling and, potentially, an activator of GATA4 activity, in conjunction with a known
481 JNK inhibitor, led to an increase in EE marker expression and EE cell number, compared with
482 G2D12 alone. We had similar findings when using a well-described inhibitor of FOXO1, which
483 has been previously implicated in beta cell differentiation[39], but whose role in EE cell
484 differentiation from primary human ISCs has not been closely examined. These protocols
485 showed high levels of human EE cell differentiation compared with prior reports[9,16,23]. While
486 transgenic over-expression of *NEUROG3* generated elevated levels of human EE cells[14,18,19],
487 our methods avoid the use of genetic techniques while maintaining EE marker expression at

488 levels at or above endogenous levels within the human duodenal mucosa. Interestingly, both
489 RSP and AS treatments also led to increased levels of *LGR5* expression, suggesting some
490 induction of stemness. It has been suggested that EE cells can act as facultative stem cells in
491 the setting of stress and injury[61], which in our organoid system may result from chronic culture
492 and/or loss of Matrigel integrity.
493
494 It is notable that two recent scRNA-seq studies analyzing human and murine EE lineage
495 differentiation using inducible expression of neurogenin 3 did not identify GATA4, JNK, or
496 FOXO1 as potential regulatory factors[15,18], suggesting that they may work upstream of
497 neurogenin 3. This is supported by increased expression of *ATOH1*, a known secretory
498 progenitor marker critical for neurogenin 3 expression[62,63], in RSP and AS enteroids
499 (Supplementary Figs 2c and 3b). It is also possible that Rim, SP, and AS are all having off
500 target effects in our enteroid model. For example, while Rim is structurally identical to a
501 described GATA4-NKX2-5 transcriptional activator[45] and induces increased expression of *GIP*
502 and *CCK*, known targets of GATA4[25-28], studies have shown that GATA4 is only expressed in
503 enterocytes of the murine duodenum[64]. It is possible that Rim is inducing GATA4 expression in
504 cells, like progenitor or EE cells, that do not normally express it. Alternatively, it is also possible
505 that GATA4 activation in other cell types, like enterocytes, is leading to the EE changes we see
506 through paracrine effects, which has been suggested in previous mouse models[27]. It might also
507 be possible that Rim is working through GATA6, which is expressed with GATA4 in the
508 duodenum[65], and is believed to have a more direct effect on EE cell differentiation[27]. In addition,
509 Rim functions as a dual inhibitor of sterol O-acyltransferase 1 (SOAT1 or ACAT1) and SOAT2
510 (ACAT2)[66], though these play more of a role in the production of steroid, not peptide,
511 hormones[67]. Finally, it is possible that Rim, acting as an inverse agonist of the CB1 receptor,
512 induces EE cell differentiation through an as yet to be identified mechanism. An additional
513 example is the use of SP600125, which did not alter PDX1 expression in our enteroid system.

514 Therefore, it is possible that JNK inhibition induces post-translational modifications on PDX1 or,
515 that in human intestinal cells, JNK inhibition does not affect PDX1. Regardless of the
516 mechanism, the use of RSP and AS induced differentiation of bona fide EE cells, as evidenced
517 by our scRNA-seq data, which showed the presence of a unique population of cells that
518 expressed EE markers and that were derived from populations of stem and progenitor cells.
519
520 Exposure of enteroids to combinations of Rim, SP, and AS led to the expression of specific
521 hormones, with RSP inducing GIP expression and AS inducing higher levels of 5HT expression.
522 Exposure to AS→RSP yielded similar levels of *GIP* mRNA and total GIP-positive enteroids, but
523 increased levels of GIP secretion, when compared to RSP alone; however, AS→RASP
524 seemingly inhibited GIP protein production and secretion. AS alone appears to be the most
525 potent inducer of 5HT secretion. Exposure to RSP, with or without AS, induced less 5HT
526 secretion when compared to AS alone. Taken together, these combinatorial data suggest that
527 AS exposure is a potent inducer of 5HT secretion while inhibiting GIP secretion, and exposure
528 to Rim and SP is a potent inducer of GIP secretion while leading to reduced 5HT secretion
529 when compared to AS treated enteroids. These data suggest that modulation of JNK, FOXO1,
530 and possibly GATA4, as well as other potential targets, could have multiple effects on EE
531 function, controlling mRNA and protein production, as well as secretion, of multiple hormones.
532
533 In comparison to enteroids, rectoids showed a much stronger induction of EE cells when
534 exposed to G2D12. It is clear that human small intestinal and colonic crypts demonstrate distinct
535 gene expression profiles, which includes genes involved in epithelial cell differentiation[68], so it is
536 likely that the requirements for EE cell lineage differentiation will be different between the
537 various regions. Additional experiments examining whether the mechanisms defined for
538 duodenal EE differentiation also regulate rectal EE differentiation need to be explored.

539

540 In summary, we have shown robust differentiation of human EE cells from duodenal and rectal
541 ISCs using Wnt3a-containing differentiation media, and, with respect to enteroids, the addition
542 of the small molecules rimonabant, SP600125, and AS1842856. These protocols improve upon
543 current methods of EE cell differentiation without the use of direct genetic alteration. These
544 studies also provide a platform for future experiments designed to identify endogenous factors
545 regulating EE differentiation, identifying the role and response of EE cells in human GI disease,
546 and further increasing EE cell numbers to potentially be used as personalized cell therapy.

547 **ONLINE METHODS**

548 **Isolation of human intestinal crypts**

549 Tissues were procured as previously described[69]. In short, de-identified endoscopic and rectal
550 biopsies were collected from grossly unaffected tissues in adolescent/young adult patients
551 undergoing esophagogastroduodenoscopy and colonoscopy at Boston Children's Hospital for
552 gastrointestinal complaints and used for organoid derivation. Further, de-identified duodenal
553 resections were collected from adult patients undergoing pancreaticoduodenectomy at
554 Massachusetts General Hospital prior to chemotherapy or radiation therapy for pancreatic
555 carcinoma. Whole mucosal biopsies were generated from the duodenal resections using
556 endoscopic biopsy forceps and used for total RNA isolation. Age and sex of donors can be
557 found in Supplementary Table 2 but were unknown to researchers when experiments were
558 being performed. Only macroscopically normal-appearing tissue was used from patients without
559 a known gastrointestinal diagnosis. Each experiment was performed on at least three
560 independent organoid lines derived from adolescent/young adult biopsy samples. Informed
561 consent and developmentally appropriate assent were obtained at Boston Children's Hospital
562 from the donors' guardian and the donor, respectively. Informed consent was obtained at
563 Massachusetts General Hospital from the donors. All methods were approved and carried out in
564 accordance with the Institutional Review Boards of Boston Children's Hospital (Protocol number
565 IRB-P00000529) and Massachusetts General Hospital (Protocol number IRB-2003P001289).
566

567 Resections were briefly washed with pre-warmed DMEM/F12, after which the epithelial layer
568 was separated from the rest of the duodenum manually with sterilized surgical tools then taken
569 for RNA isolation. To isolate crypts, adolescent/young adult biopsies were digested in 2 mg/mL
570 of Collagenase Type I reconstituted in Hank's Balanced Salt Solution for 40 minutes at 37°C.
571 Samples were then agitated by pipetting followed by centrifugation at 500 x g for 5 minutes at

572 4°C. The supernatant was then removed, and crypts resuspended in 200-300 µL of Matrigel,
573 with 50µL being plated onto 4-6 wells of a 24-well plate and polymerized at 37°C.
574
575 **Culturing of human duodenal and rectal organoids *in vitro***
576 Isolated crypts in Matrigel were grown in specific growth media (GM) (Supplementary Table 1)
577 based on the tissue of origin. The resulting organoids were passaged every 6-8 days as
578 needed, with media changes occurring every two days. To passage, Matrigel was mechanically
579 dissociated from the well and resuspended in 500 µL of Cell Recovery solution for 40-60
580 minutes at 4°C. To aid in separating the Matrigel and enteroids, the tubes are gently inverted
581 and then centrifuged at 500 x g for 5 minutes at 4°C. The supernatant was then removed, and
582 organoids resuspended in Matrigel, followed by mechanical disruption via a bent-tipped pipette.
583 Organoids were passaged at a 1:2 dilution, with 50 µL per well of a 24-well plate. After plating,
584 the organoids were incubated at 37°C for 10 minutes to allow the Matrigel to set. Once
585 complete, 500 µL of GM was added to each well.
586
587 For differentiation, organoids were passaged and grown in GM for two days, to allow for ISC
588 expansion, after which the organoids were transitioned to tissue-specific differentiation media
589 (DM) with additional small molecules added as described (Supplementary Table 1). Media was
590 changed every two days, with Tubastatin A being removed after the second day of
591 differentiation. Enteroid and rectoids were taken for analysis after 14 days.
592
593 **Gene expression analysis**
594 Total RNA was purified from individual wells using TRI®Reagent and the Direct-zol™ RNA kit,
595 following the manufacturer's protocol. RNA concentration was determined using a NanoDrop™
596 1000 spectrophotometer (Life Technologies). RNA was then reverse transcribed using the High-

597 Capacity cDNA Reverse Transcription Kit. Gene expression analysis was then performed by
598 Real Time quantitative PCR (qPCR) using a QuantStudio 6 Flex thermocycler (Thermo Fisher).
599 We used the following Taqman primers from Thermo Fisher (Supplementary Table 3). *18S*
600 transcripts were used as the internal control and data were expressed using the 2^{-ddCt} method
601 with Ct limit of 40. Fold change, unless otherwise stated, was compared to total RNA derived
602 from whole mucosal tissue biopsies, using duodenal mucosa with enteroids and rectal mucosa
603 with rectoids.
604
605 **DNA isolation**
606 To isolate organoid genomic DNA, 200 µL of 50 mM NaOH was added to a single well of a 24-
607 well plate and the Matrigel was mechanically dissociated. The samples were then transferred to
608 1.5 mL microcentrifuge tubes and placed in a 95°C heat block for 20 minutes. The tubes were
609 then vortexed, after which 25 µL of 1M Tris-HCl was added. The samples were then centrifuged
610 at 14,000 rpm for 10 minutes. The DNA content of the supernatant was then assayed using a
611 NanoDrop™ 1000 spectrophotometer (Thermo Fisher).
612
613 **Immunofluorescence**
614 Immunofluorescence staining was performed as previously described with minor
615 modifications[70]. Organoids were grown in and isolated from Matrigel as noted above. 1-3 wells
616 from a 24-well plate were washed in 200 µL of 1X phosphate-buffered saline (PBS) and moved
617 in suspension to a 1.5 mL microcentrifuge tube. Each tube was centrifuged at 800 x g for 5
618 minutes at 4°C to pellet organoids. PBS was aspirated, and organoids were fixed in 200 µL of
619 4% paraformaldehyde (PFA) for 20 minutes on ice, shaking. Each tube was centrifuged again
620 as above, and PFA was aspirated. The organoids were then resuspended in 500 µL of 0.3%
621 Triton-X in PBS and moved to a 48-well plate for the remaining steps. The organoids were

622 permeabilized for 30 minutes at room temperature, shaking. Between each step, organoids
623 were allowed to settle to the bottom of each well, the plate was angled, and the solution
624 aspirated by careful pipetting. Organoids were then blocked with 5% bovine serum albumin
625 (BSA) in PBS for 1.5 hours at room temperature, shaking. This was followed by three five-
626 minute washes in 500 µL of PBS at room temperature, shaking.
627
628 Each well was then incubated in 200 µL of primary antibodies diluted in 5% BSA/0.1% Trition-X
629 in PBS at 4°C overnight. This was followed by five washes in 500 µL of 0.1% Triton-X in PBS for
630 15 minutes each at room temperature, shaking. 200 µL of secondary antibodies diluted in 0.1%
631 Triton-X in PBS were then added to each well and incubated for two hours at room temperature,
632 shaking. Organoids were then washed as above, then moved to new 1.5 mL centrifuge tubes.
633 During the last wash, 4′,6-diamidino-2-phenylindole (DAPI) was added at a concentration of
634 1:1000 for nuclear staining. Organoids were then centrifuged at 1000 x g for 5 minutes at 4°C to
635 help remove as much PBS as possible. Slides were prepared by drawing three circles with a
636 hydrophobic pen. Enteroids were then resuspended in 20 µL of Prolong Gold Antifade mountant
637 and droplets placed within hydrophobic circles. The organoids were spread out to reduce
638 clumping, sealed with a coverslip, and allowed to dry overnight at room temperature. Slides
639 were stored at 4°C for future imaging. Images were acquired using a Nikon upright Eclipse 90i
640 microscope with a 20×/0.75 Plan-Apochromat objective and adjusted for brightness and
641 contrast in Fiji[71].
642
643 **Quantification of enteroid immunofluorescence**
644 This technique was adapted from a previously described method[72]. Immunofluorescent images
645 were acquired using an Invitrogen EVOS FL 2 Auto microscope (Thermo Fisher).
646 Representative images of stained organoids were taken at 2X magnification. The stitched

647 images were then processed in Fiji[71]. The color of the DAPI images was converted to 8-bit
648 grayscale and then the image was smoothed by applying a Gaussian Blur filter (radius = 4,
649 scaled units). Thresholding of the smoothed images was performed using manual adjustment to
650 achieve optimal separation of individual organoids. Watershed and Find Edges filters were then
651 applied to segment any clumped organoids. Post-segmentation analysis was performed to
652 outline and count individual organoids using Analyze Particles (size=4,000-100,000,
653 circularity=0.30-1.00, exclude on edges). Each image was then manually curated to exclude
654 debris and organoids exhibiting background fluorescence. Any remaining clumped organoids
655 were manually separated prior to quantification. The outlines generated from the DAPI images
656 were then applied to the corresponding images from the other fluorescent channels. Each color
657 image was converted to 8-bit grayscale and then the HiLo Lookup Table was applied. The
658 threshold gate for stained cells was found by manual adjustment of positively stained organoids
659 to achieve optimal representation. The threshold gate for each channel was then applied to
660 each experimental condition. The Mean metric was extracted with ROI manager (measure) and
661 compiled for analysis. Organoids with a Mean value of more than zero were considered positive.
662

663 **Flow cytometry**

664 Organoids were incubated in Cell Recovery solution for 40-60 minutes at 4°C to remove the
665 Matrigel and then centrifuged at 500 x g for 5 minutes at 4°C. To achieve single cell suspension,
666 organoids were then incubated in 500 µL of TrypLE Express at 37°C for 30 minutes and broken
667 up by repeated pipetting using a bent P1000 pipette tip. Each sample was then diluted in 800µL
668 of 20% fetal bovine serum (FBS) in Advanced DMEM/F12 and then centrifuged at 800 x g for 5
669 minutes at 4°C. To mark dead cells, each sample was then incubated in DAPI (1:1000) diluted
670 in 2% FBS/2 mM EDTA/calcium-free DMEM for 20 minutes at room temperature, then
671 centrifuged at 800 x g for 5 minutes at 4°C and washed in 2% FBS/2 mM EDTA/DMEM. Cells

672 were then incubated in 1% PFA for 15 minutes at room temperature, washed with 2% FBS/PBS
673 and then permeabilized in 0.2% Tween 20 in 2% FBS/PBS for 15 minutes at 37°C. Following
674 centrifugation, cells were resuspended in 0.1% Tween 20/2% FBS/2 mM EDTA in PBS with
675 PE/Alexa Fluor 647-conjugated CHGA, PE-conjugated mouse IgG1, K isotype, Alexa Fluor 647-
676 conjugated mouse IgG2b, K isotype, or with no antibody (the latter three acting as controls) for
677 30 minutes on ice. Cells were then washed in 0.1% Tween 20/2% FBS/2 mM EDTA in PBS,
678 filtered through a 37-micron mesh, and then analyzed on a BD FACSAria II SORP flow
679 cytometer. For gating strategy, please see Supplementary Figure 10.
680
681 **Cell proliferation**
682 Enteroid cell proliferation was assessed using the Click-IT EdU Alexa Fluor 488 Flow Cytometry
683 Assay kit following the manufacturer's protocols. Briefly, enteroids were grown in Matrigel as
684 noted above and taken for analysis after 7 and 14 days. Enteroids were labeled following
685 incubation with 10 μM of EdU at 37°C for 2 hours and then incubated with TrypLE Express as
686 above to isolate single cells. All samples were then diluted in 800 μL of 20% FBS in Advanced
687 DMEM/F12 and then centrifuged at 800 x g for 5 minutes at 4°C. Fixation, permeabilization, and
688 the Click-iT reaction were performed in accordance with manufacturer's protocols before being
689 filtered through a 37-micron mesh, and then analyzed on a BD FACSAria II SORP flow
690 cytometer.
691
692 **Cell apoptosis**
693 Apoptosis was assessed using the Dead Cell Apoptosis Kit with Annexin V Alexa Fluor 488 &
694 Propidium Iodide following the manufacturer's protocols. For these experiments, enteroids were
695 grown in Matrigel as noted above and taken for analysis after 7 and 14 days. To isolate single
696 cells, enteroids were incubated with TrypLE Express as above. All samples were then diluted in

697 800 µL of 20% FBS in Advanced DMEM/F12 and then centrifuged at 800 x g for 5 minutes at
698 4°C. Samples were then incubated with propidium iodide and annexin V per manufacturer's
699 protocol. Cells were filtered through a 37-micron mesh, and then analyzed on a BD FACSAria II
700 SORP flow cytometer.
701
702 **ELISA**
703 Hormone quantification for 5HT, GIP, GLP-1, and PYY were performed using kits and following
704 the manufacturer's protocols. For these experiments, organoids were grown in 48-well plates to
705 aid in concentrating the hormone of interest. Conditioned media was taken on day 14 of
706 differentiation, 48 hours after last media change. Diprotin A (100µM), a dipeptidyl peptidase 4
707 inhibitor, was added daily to the media for the last two days of differentiation to prevent GIP and
708 GLP-1 degradation. For hormone induction studies, conditioned media was taken on day 13, 24
709 hours after last media change, after which forskolin (10 µM) was added to fresh media and
710 collected after 24 hours. As an additional control, differentiation media not exposed to cells was
711 also evaluated. This value was then subtracted from each experimental sample.
712
713 **Sample Preparation for single cell RNA sequencing**
714 Enteroids were incubated in Cell Recovery solution for 40-60 minutes at 4°C to remove the
715 Matrigel and then centrifuged at 500 x g for 5 minutes at 4°C. To achieve single cell suspension,
716 organoids were then incubated in 500 µL of TrypLE Express at 37°C for 30 minutes and broken
717 up by repeated pipetting using a bent P1000 pipette tip. Each sample was then diluted in 800 µL
718 of 20% FBS in Advanced DMEM/F12, filtered through 37 µm mesh, and then centrifuged at 300
719 x g for 10 minutes at 4°C. Dead cells were then removed using MACS separation following the
720 manufacturer's protocol. Briefly, each sample was resuspended in 100 µL Dead Cell Removal
721 MicroBeads and incubated at room temperature for 15 minutes. Four hundred microliters of 1x

722 Binding Buffer were then added to each sample, after which the samples were applied to
723 prepared MACS columns placed in a MACS Separator. Flow-through containing live cells was
724 collected. This was followed by washing the columns four times with 1x Binding Buffer, which
725 were combined with the initial flow-through. These samples were then centrifuged at 800 x g for
726 5 minutes at 4°C.
727
728 **Hashtag-labeling of sequencing samples**
729 Single cells isolated after dead cell removal were labeled prior to sequencing with Biolegend
730 Totalseq-B hashtag antibodies, targeted against CD298 and β2-microglobulin, per the
731 manufacturer's protocol[47]. Briefly, each of the nine samples (three separate differentiation
732 conditions in three enteroid lines) were resuspended in 50 µL of Cell Staining Buffer and
733 blocked with 5 µL of Human TruStain FcX™ blocking reagent for 10 minutes at 4°C. The
734 supernatant was then removed, and each sample resuspended in 50 µL of Cell Staining Buffer
735 containing 1 µg of a unique Totalseq-B hashtag antibody. Samples were incubated for 30
736 minutes at 4°C and then washed three times in 3.5 mL of Cell Staining Buffer. The samples
737 were then filtered through a 37 µm mesh, resuspended in 2% BSA in PBS at a concentration of
738 1500 cells/µL, and then pooled together. Of note, prior to the scRNA-seq experiment, antibody
739 binding was verified using fluorophore-conjugated antibodies with the same binding specificity.
740
741 **Droplet-based single cell RNA sequencing and alignment**
742 A total of 180,000 cells as one pool were input across four channels, with a recovery rate of
743 approximately 30,000 cells across all four channels. RNA libraries were prepared from single
744 cells by the Single Cell Core at Harvard Medical School, Boston, MA, using the 10X Chromium
745 Single Cell 3' Library Chip (V3.1) with dual indexed barcodes. Briefly, single cells were
746 partitioned into Gel Beads in Emulsion (GEMs) by the Chromium Controller. Prior to partitioning,

747 hashed cells were pooled together and “super-loaded” to reduce batch effects across
748 samples[47]. Once partitioned, cells were lysed and RNA was captured, reverse transcribed, and
749 amplified. cDNA was then enzymatically fragmented and sample indices were attached to both
750 ends of the fragment. Following library prep, the transcriptomes were sequenced by the
751 Molecular Biology Core Facilities at the Dana-Farber Cancer Institute on an Illumina NovaSeq
752 6000 sequencing platform. The pooled sample was split across two lanes on a NovaSeq S1
753 flow cell.
754
755 After sequencing, the files were processed, demultiplexed and aligned using 10X’s Cell Ranger
756 software (v5.0.1). Briefly, raw BCL files were demultiplexed using the cellranger mkfastq
757 function, a wrapper of Illumina’s bcl2fastq, with the filter dual index argument set to true.
758 Following the generation of the FASTQ files, the samples were aligned to the hg19 human
759 genome and features were counted using the cellranger count function. This function aligned
760 the UMIs of each individual cell to the related gene and counted the number of detected UMIs to
761 generate a feature-barcode matrix. In addition, it also measured the hashtag oligo counts for
762 each individual cell from the relevant hashtag antibodies that were used to label each condition.
763 Further, for analysis of RNA velocity, both un-spliced and spliced RNA variants were aligned
764 and counted using the velocyto.py package (v0.17.16)[56].
765
766 **Single cell RNA sequencing analysis**
767 Analysis of the scRNA-seq data was conducted using the Seurat package (v4.0.1), within the R
768 programming language (v4.0.3). Initially, cells were filtered to only include those with at least
769 one detectable hashtag antibody signal, and then hashtag counts were normalized, and the cell
770 samples were demultiplexed using the HTOdemux function built into Seurat. This function
771 ranked a cell as being positive for a specific hashtag signal, if the detected signal was in the

772 99th percentile or higher. Cells were then demultiplexed, with cells that had no positive signals
773 being labeled as negative cells, cells with only one positive signal being labeled by their
774 respective positive signal, and cells with two or more positive signals being labeled as doublets.
775 Following demultiplexing, the dataset was pre-processed to remove cells that were deemed of
776 lower quality, based on their number of unique genes (<200 unique genes) and the proportion of
777 UMIs that corresponded to mitochondrial RNA (>25% of UMIs)[48].
778
779 After the removal of doublet barcodes, negative barcodes and the remaining barcodes that were
780 deemed to be of lower quality, we were left with a combined dataset of 14,767 cells that was
781 used for further analysis. To better control for batch effects and to improve our ability to detect
782 diversity within our samples, we normalized the gene counts using regularized negative
783 binomial regression, using SCTransform[73]. Following normalization, we performed dimensional
784 reduction by running Principal Component Analysis (PCA) and, based on the elbow plot
785 generated, selected the first 20 principal components for defining the K nearest neighbors and
786 the UMAP plot. After dimensional reduction, 15 clusters were defined using Louvain clustering
787 (resolution=0.5). Differentially expressed genes were identified across each cluster using the
788 Wilcoxon rank sum test via the FindAllMarkers function built into Seurat. Only genes that were
789 expressed in at least 25% of cells and had a log-fold change of 0.25 were considered in this
790 analysis. These differential genes, as well as classical epithelial markers, were used to broadly
791 categorize the clusters into six epithelial cell types and include *LGR5, AXIN2* and *ASCL2* for
792 intestinal stem cells, *KRT20*, *FABP2*, and *FABP1* for enterocytes, *MUC2, FCGBP,* and *GFI1* for
793 goblet cells, *CHGA*, *NEUROG3*, *NEUROD1* and *PAX4* for enteroendocrine cells, *CD44* for
794 progenitor cells and *MKI67* for proliferating cells[51-53].
795
796 Finally, enteroid EE cell identity was compared to the gene set signature from tissue EE cells
797 isolated from the murine small intestine[49]. To compare the gene signature, we calculated the

gene module score of each individual cell using the AddModuleScore function found in Seurat v3 and v4, which calculates the score based on the enrichment of the specified gene set compared to randomly selected genes with a comparable average gene expression[48]. The AddModuleScore function calculates a scaled score between 0 to 1.

Trajectory analysis with scVelo

RNA velocity was calculated using the scVelo package (v0.2.3) with Scanpy (v1.7.1) on Python (v3.7.9)[55]. To perform trajectory analysis, the un-spliced and spliced variant count matrix that was previously calculated using velocyto was fused with an anndata object containing the UMAP information and cluster identities defined in Seurat analysis. The combined dataset was then processed using the scVelo pipeline: The ratio of un-spliced:spliced RNA for each gene was normalized and filtered using the default settings. Afterwards, the first and second moments were calculated for velocity estimation. Following moment calculation, the dynamic model was used to calculate the RNA velocities. The dynamic model iteratively estimates the parameters that best model the phase trajectory of each gene, therefore capturing the most accurate, albeit more computationally intensive, estimate of the dynamics for each gene. These approaches were used to graphically model the RNA velocity for each culture condition.

Quantification and statistical analysis

All experiments were repeated using at least three different human organoid lines and representative data from a single line is shown. For qPCR and flow cytometry studies, each condition was performed using pooled enteroids from 3-5 wells, unless otherwise noted, with each well acting as a single sample. Whole mucosal biopsies from duodenal resections and whole mucosa rectal biopsies were combined from three different individuals to generate a single reference sample for all enteroid and rectoid experiments.

824 Prior to statistical analysis, all qPCR data were transformed using $\log_{10}$. When analyzing only
825 two conditions, statistical significance was determined by unpaired, two-tailed Student's *t* test,
826 combined with the Holm-Sidak method to control for multiple comparisons. When analyzing
827 more than two conditions, statistical significance was determined by either one-way or two-way
828 ANOVA, followed by Tukey post hoc analysis. Specific conditions were excluded from statistical
829 analysis if the data from one or more samples was labeled as not detectable. When analyzing
830 the statistical relationship between cell proportions identified using single cell RNA sequencing,
831 the non-parametric Kruskal-Wallis test was conducted, followed by Dunn's post-hoc analysis.
832 We used the Bonferroni correction to account for multiple hypothesis testing when performing
833 the post-hoc analysis. When comparing the distribution of gene module scores across the three
834 different culture conditions, effect size was used to compare large changes and was calculated
835 as Cohen's d. Statistical details for each experiment can be found within each figure legend.
836
837 **Reagents**
838 A list of all resources used in this study, including source and catalog number, can be found in
839 Supplementary Table 4.
840
841 **ACKNOWLEDGEMENTS**
842 We thank members of the Breault laboratory, J. Majzoub, S. Bonner-Weir and J. Turner for
843 helpful discussions. This research was supported by National Institute of Health (NIH) awards
844 T32DK769937, K12DK09472109, the Juvenile Diabetes Research Foundation Advanced
845 Postdoctoral Fellowship award 3-APF-2020-929-A-N, and Pediatric Endocrine Society
846 Research Fellowship and Clinical Scholar Awards (to D.Z.), NIH awards HL095722 and
847 UC4DK104165 (to J.M.K.), and NIH awards DK119488 and DK034854 and support from the
848 Adolph Coors Foundation (to D.T.B.).
849

AUTHOR CONTRIBUTIONS

D.Z. designed and performed experiments, analyzed data, prepared figures and co-wrote the manuscript; E.S., P.M., and W.Q. performed experiments, analyzed data and edited the manuscript; J.S.C. performed and analyzed the single cell RNA sequencing experiment; X.Y. and E.P.S. performed cell culture experiments; M.S.S. performed flow cytometry experiments; S.D. and S.H. assisted in qPCR and immunofluorescence experiments; J.M.K. provided conceptual advice and reagents; D.L.C. and J.O.M. provided conceptual advice and edited the manuscript, and D.T.B. directed the project and co-wrote the manuscript.

COMPETING INTERESTS

The author J.M.K. holds equity in Frequency Therapeutics, a company that has an option to license IP generated by J.M.K and that may benefit financially if the IP is licensed and further validated. The interests of J.M.K. was reviewed and are subject to a management plan overseen by their institutions in accordance with their conflict-of-interest policies.

Data Availability

Data generated in this study have been deposited in Gene Expression Omnibus with the accession code: “(pending)”. All other relevant data supporting the key findings of this study are available within the article and its Supplementary Information files or from the corresponding author upon reasonable request.

Code Availability

This study did not generate or use any previously unreported custom code.

875 **REFERENCES**

876

877 1 Posovszky, C. Development and Anatomy of the Enteroendocrine System in Humans.
878 *Endocr Dev* **32**, 20-37, doi:10.1159/000475729 (2017).

879 2 Furness, J. B., Rivera, L. R., Cho, H. J., Bravo, D. M. & Callaghan, B. The gut as a sensory
880 organ. *Nat Rev Gastroenterol Hepatol* **10**, 729-740, doi:10.1038/nrgastro.2013.180
881 (2013).

882 3 El-Salhy, M., Hausken, T., Gilja, O. H. & Hatlebakk, J. G. The possible role of
883 gastrointestinal endocrine cells in the pathophysiology of irritable bowel syndrome. *Expert*
884 *Rev Gastroenterol Hepatol* **11**, 139-148, doi:10.1080/17474124.2017.1269601 (2017).

885 4 Worthington, J. J., Reimann, F. & Gribble, F. M. Enteroendocrine cells-sensory sentinels
886 of the intestinal environment and orchestrators of mucosal immunity. *Mucosal Immunol*
887 **11**, 3-20, doi:10.1038/mi.2017.73 (2018).

888 5 Holst, J. J., Vilsboll, T. & Deacon, C. F. The incretin system and its role in type 2 diabetes
889 mellitus. *Mol Cell Endocrinol* **297**, 127-136, doi:10.1016/j.mce.2008.08.012 (2009).

890 6 Yousefi, M., Li, L. & Lengner, C. J. Hierarchy and Plasticity in the Intestinal Stem Cell
891 Compartment. *Trends Cell Biol* **27**, 753-764, doi:10.1016/j.tcb.2017.06.006 (2017).

892 7 Yu, H. *et al.* The Contributions of Human Mini-Intestines to the Study of Intestinal
893 Physiology and Pathophysiology. *Annu Rev Physiol* **79**, 291-312, doi:10.1146/annurev-
894 physiol-021115-105211 (2017).

895 8 Fujii, M. *et al.* Human Intestinal Organoids Maintain Self-Renewal Capacity and Cellular
896 Diversity in Niche-Inspired Culture Condition. *Cell Stem Cell* **23**, 787-793 e786,
897 doi:10.1016/j.stem.2018.11.016 (2018).

898 9 Sato, T. *et al.* Long-term expansion of epithelial organoids from human colon, adenoma,
899 adenocarcinoma, and Barrett's epithelium. *Gastroenterology* **141**, 1762-1772,
900 doi:10.1053/j.gastro.2011.07.050 (2011).

901 10 Basak, O. *et al.* Induced Quiescence of Lgr5+ Stem Cells in Intestinal Organoids Enables
902 Differentiation of Hormone-Producing Enteroendocrine Cells. *Cell Stem Cell* **20**, 177-190
903 e174, doi:10.1016/j.stem.2016.11.001 (2017).

904 11 Sato, T. & Clevers, H. SnapShot: Growing Organoids from Stem Cells. *Cell* **161**, 1700-
905 1700 e1701, doi:10.1016/j.cell.2015.06.028 (2015).

906 12 Yin, X. *et al.* Niche-independent high-purity cultures of Lgr5+ intestinal stem cells and their
907 progeny. *Nat Methods* **11**, 106-112, doi:10.1038/nmeth.2737 (2014).

908 13 Almeqdadi, M., Mana, M. D., Roper, J. & Yilmaz, O. H. Gut organoids: mini-tissues in
909 culture to study intestinal physiology and disease. *Am J Physiol Cell Physiol* **317**, C405-
910 C419, doi:10.1152/ajpcell.00300.2017 (2019).

911 14 Sinagoga, K. L. *et al.* Deriving functional human enteroendocrine cells from pluripotent
912 stem cells. *Development* **145**, doi:10.1242/dev.165795 (2018).

913 15 Gehart, H. *et al.* Identification of Enteroendocrine Regulators by Real-Time Single-Cell
914 Differentiation Mapping. *Cell* **176**, 1158-1173 e1116, doi:10.1016/j.cell.2018.12.029
915 (2019).

916 16 Beumer, J. *et al.* Enteroendocrine cells switch hormone expression along the crypt-to-
917 villus BMP signalling gradient. *Nat Cell Biol* **20**, 909-916, doi:10.1038/s41556-018-0143-y
918 (2018).

919 17 Chen, C., Fang, R., Davis, C., Maravelias, C. & Sibley, E. Pdx1 inactivation restricted to
920 the intestinal epithelium in mice alters duodenal gene expression in enterocytes and
921 enteroendocrine cells. *Am J Physiol Gastrointest Liver Physiol* **297**, G1126-1137,
922 doi:10.1152/ajpgi.90586.2008 (2009).

923 18 Beumer, J. *et al.* High-Resolution mRNA and Secretome Atlas of Human Enteroendocrine
924 Cells. *Cell* **181**, 1291-1306 e1219, doi:10.1016/j.cell.2020.04.036 (2020).

925 19 Chang-Graham, A. L. *et al.* Human Intestinal Enteroids With Inducible Neurogenin-3
926 Expression as a Novel Model of Gut Hormone Secretion. *Cell Mol Gastroenterol Hepatol*
927 **8**, 209-229, doi:10.1016/j.jcmgh.2019.04.010 (2019).

928 20 Munera, J. O. *et al.* Differentiation of Human Pluripotent Stem Cells into Colonic Organoids
929 via Transient Activation of BMP Signaling. *Cell Stem Cell* **21**, 51-64 e56,
930 doi:10.1016/j.stem.2017.05.020 (2017).

931 21 McCracken, K. W. *et al.* Modelling human development and disease in pluripotent stem-
932 cell-derived gastric organoids. *Nature* **516**, 400-404, doi:10.1038/nature13863 (2014).

933 22 Petersen, N. *et al.* Generation of L cells in mouse and human small intestine organoids.
934 *Diabetes* **63**, 410-420, doi:10.2337/db13-0991 (2014).

935 23 VanDussen, K. L. *et al.* Development of an enhanced human gastrointestinal epithelial
936 culture system to facilitate patient-based assays. *Gut* **64**, 911-920, doi:10.1136/gutjnl-
937 2013-306651 (2015).

938 24 Girard, R. *et al.* HNF4alpha is a novel regulator of intestinal glucose-dependent
939 insulinotropic polypeptide. *Sci Rep* **9**, 4200, doi:10.1038/s41598-019-41061-z (2019).

940 25 Jepeal, L. I., Boylan, M. O. & Michael Wolfe, M. GATA-4 upregulates glucose-dependent
941 insulinotropic polypeptide expression in cells of pancreatic and intestinal lineage. *Mol Cell*
942 *Endocrinol* **287**, 20-29, doi:10.1016/j.mce.2008.01.024 (2008).

943 26 Walker, E. M., Thompson, C. A. & Battle, M. A. GATA4 and GATA6 regulate intestinal
944 epithelial cytodifferentiation during development. *Dev Biol* **392**, 283-294,
945 doi:10.1016/j.ydbio.2014.05.017 (2014).

946 27 Walker, E. M., Thompson, C. A., Kohlnhofer, B. M., Faber, M. L. & Battle, M. A.
947 Characterization of the developing small intestine in the absence of either GATA4 or
948 GATA6. *BMC Res Notes* **7**, 902, doi:10.1186/1756-0500-7-902 (2014).

949 28 Kohlnhofer, B. M., Thompson, C. A., Walker, E. M. & Battle, M. A. GATA4 regulates
950 epithelial cell proliferation to control intestinal growth and development in mice. *Cell Mol*
951 *Gastroenterol Hepatol* **2**, 189-209, doi:10.1016/j.jcmgh.2015.11.010 (2016).

952 29 Biteau, B., Hochmuth, C. E. & Jasper, H. JNK activity in somatic stem cells causes loss of
953 tissue homeostasis in the aging Drosophila gut. *Cell Stem Cell* **3**, 442-455,
954 doi:10.1016/j.stem.2008.07.024 (2008).

955 30 Sancho, R. *et al.* JNK signalling modulates intestinal homeostasis and tumourigenesis in
956 mice. *EMBO J* **28**, 1843-1854, doi:10.1038/emboj.2009.153 (2009).

957 31 Kaneto, H. *et al.* Oxidative stress and the JNK pathway in diabetes. *Curr Diabetes Rev* **1**,
958 65-72 (2005).

959 32 Tang, C. *et al.* Glucose-Induced beta-Cell Dysfunction In Vivo: Evidence for a Causal Role
960 of C-jun N-terminal Kinase Pathway. *Endocrinology* **159**, 3643-3654,
961 doi:10.1210/en.2018-00566 (2018).

962 33 Mandic, A. D. *et al.* c-Jun N-terminal kinase 2 promotes enterocyte survival and goblet cell
963 differentiation in the inflamed intestine. *Mucosal Immunol* **10**, 1211-1223,
964 doi:10.1038/mi.2016.125 (2017).

965 34 Kousteni, S. FoxO1, the transcriptional chief of staff of energy metabolism. *Bone* **50**, 437-
966 443, doi:10.1016/j.bone.2011.06.034 (2012).

967 35 Tothova, Z. & Gilliland, D. G. FoxO transcription factors and stem cell homeostasis:
968 insights from the hematopoietic system. *Cell Stem Cell* **1**, 140-152,
969 doi:10.1016/j.stem.2007.07.017 (2007).

970 36 Roy, S. A. *et al.* Dual regulatory role for phosphatase and tensin homolog in specification
971 of intestinal endocrine cell subtypes. *World J Gastroenterol* **18**, 1579-1589,
972 doi:10.3748/wjg.v18.i14.1579 (2012).

973 37 Garcia-Martinez, J. M., Chocarro-Calvo, A., De la Vieja, A. & Garcia-Jimenez, C. Insulin
974 drives glucose-dependent insulinotropic peptide expression via glucose-dependent
975 regulation of FoxO1 and LEF1/beta-catenin. *Biochim Biophys Acta* **1839**, 1141-1150,
976 doi:10.1016/j.bbagrm.2014.07.020 (2014).

977 38 Arriola, D. J., Mayo, S. L., Skarra, D. V., Benson, C. A. & Thackray, V. G. FOXO1
978 transcription factor inhibits luteinizing hormone beta gene expression in pituitary
979 gonadotrope cells. *J Biol Chem* **287**, 33424-33435, doi:10.1074/jbc.M112.362103 (2012).

980 39 Bouchi, R. *et al.* FOXO1 inhibition yields functional insulin-producing cells in human gut
981 organoid cultures. *Nat Commun* **5**, 4242, doi:10.1038/ncomms5242 (2014).

982 40 DiPatrizio, N. V. Endocannabinoids in the Gut. *Cannabis Cannabinoid Res* **1**, 67-77,
983 doi:10.1089/can.2016.0001 (2016).

984 41 Pagliuca, F. W. *et al.* Generation of functional human pancreatic beta cells in vitro. *Cell*
985 **159**, 428-439, doi:10.1016/j.cell.2014.09.040 (2014).

986 42 Harskamp, L. R., Gansevoort, R. T., van Goor, H. & Meijer, E. The epidermal growth factor
987 receptor pathway in chronic kidney diseases. *Nat Rev Nephrol* **12**, 496-506,
988 doi:10.1038/nrneph.2016.91 (2016).

989 43 Zhao, X., Mohan, R., Ozcan, S. & Tang, X. MicroRNA-30d induces insulin transcription
990 factor MafA and insulin production by targeting mitogen-activated protein 4 kinase 4
991 (MAP4K4) in pancreatic beta-cells. *J Biol Chem* **287**, 31155-31164,
992 doi:10.1074/jbc.M112.362632 (2012).

993 44 Sathyapalan, T. *et al.* Effect of rimonabant and metformin on glucose-dependent
994 insulinotropic polypeptide and glucagon-like peptide-1 in obese women with polycystic
995 ovary syndrome. *Clin Endocrinol (Oxf)* **72**, 423-425, doi:10.1111/j.1365-
996 2265.2009.03643.x (2010).

997 45 Valimaki, M. J. *et al.* Discovery of Small Molecules Targeting the Synergy of Cardiac
998 Transcription Factors GATA4 and NKX2-5. *J Med Chem* **60**, 7781-7798,
999 doi:10.1021/acs.jmedchem.7b00816 (2017).

1000 46 Yu, F. *et al.* FoxO1 inhibition promotes differentiation of human embryonic stem cells into
1001 insulin producing cells. *Exp Cell Res* **362**, 227-234, doi:10.1016/j.yexcr.2017.11.022
1002 (2018).

1003 47 Stoeckius, M. *et al.* Cell Hashing with barcoded antibodies enables multiplexing and
1004 doublet detection for single cell genomics. *Genome Biol* **19**, 224, doi:10.1186/s13059-018-
1005 1603-1 (2018).

1006 48 Stuart, T. *et al.* Comprehensive Integration of Single-Cell Data. *Cell* **177**, 1888-1902
1007 e1821, doi:10.1016/j.cell.2019.05.031 (2019).

1008 49 Haber, A. L. *et al.* A single-cell survey of the small intestinal epithelium. *Nature* **551**, 333-
1009 339, doi:10.1038/nature24489 (2017).

1010 50 Mead, B. E. *et al.* Harnessing single-cell genomics to improve the physiological fidelity of
1011 organoid-derived cell types. *BMC Biol* **16**, 62, doi:10.1186/s12915-018-0527-2 (2018).

1012 51 Barker, N. Adult intestinal stem cells: critical drivers of epithelial homeostasis and
1013 regeneration. *Nat Rev Mol Cell Biol* **15**, 19-33, doi:10.1038/nrm3721 (2014).

1014 52 van der Flier, L. G. & Clevers, H. Stem cells, self-renewal, and differentiation in the
1015 intestinal epithelium. *Annu Rev Physiol* **71**, 241-260,
1016 doi:10.1146/annurev.physiol.010908.163145 (2009).

1017 53 Noah, T. K., Donahue, B. & Shroyer, N. F. Intestinal development and differentiation. *Exp*
1018 *Cell Res* **317**, 2702-2710, doi:10.1016/j.yexcr.2011.09.006 (2011).

1019 54 Basak, O. *et al.* Mapping early fate determination in Lgr5+ crypt stem cells using a novel
1020 Ki67-RFP allele. *EMBO J* **33**, 2057-2068, doi:10.15252/embj.201488017 (2014).

1021 55 Bergen, V., Lange, M., Peidli, S., Wolf, F. A. & Theis, F. J. Generalizing RNA velocity to
1022 transient cell states through dynamical modeling. *Nat Biotechnol* **38**, 1408-1414,
1023 doi:10.1038/s41587-020-0591-3 (2020).

1024 56 La Manno, G. *et al.* RNA velocity of single cells. *Nature* **560**, 494-498,
1025 doi:10.1038/s41586-018-0414-6 (2018).

1026 57 Asfaha, S. *et al.* Krt19(+)/Lgr5(-) Cells Are Radioresistant Cancer-Initiating Stem Cells in
1027 the Colon and Intestine. *Cell Stem Cell* **16**, 627-638, doi:10.1016/j.stem.2015.04.013
1028 (2015).

1029 58 Tetteh, P. W. *et al.* Replacement of Lost Lgr5-Positive Stem Cells through Plasticity of
1030 Their Enterocyte-Lineage Daughters. *Cell Stem Cell* **18**, 203-213,
1031 doi:10.1016/j.stem.2016.01.001 (2016).

1032 59 Bekku, S. *et al.* Carbonic anhydrase I and II as a differentiation marker of human and rat
1033 colonic enterocytes. *Res Exp Med (Berl)* **198**, 175-185, doi:10.1007/s004330050101
1034 (1998).

1035 60 Gonzalez, L. M., Williamson, I., Piedrahita, J. A., Blikslager, A. T. & Magness, S. T. Cell
1036 lineage identification and stem cell culture in a porcine model for the study of intestinal
1037 epithelial regeneration. *PLoS One* **8**, e66465, doi:10.1371/journal.pone.0066465 (2013).

1038 61 Yan, K. S. *et al.* Intestinal Enteroendocrine Lineage Cells Possess Homeostatic and Injury-
1039 Inducible Stem Cell Activity. *Cell Stem Cell* **21**, 78-90 e76, doi:10.1016/j.stem.2017.06.014
1040 (2017).

1041 62 Shroyer, N. F. *et al.* Intestine-specific ablation of mouse atonal homolog 1 (Math1) reveals
1042 a role in cellular homeostasis. *Gastroenterology* **132**, 2478-2488,
1043 doi:10.1053/j.gastro.2007.03.047 (2007).

1044 63 Yang, Q., Bermingham, N. A., Finegold, M. J. & Zoghbi, H. Y. Requirement of Math1 for
1045 secretory cell lineage commitment in the mouse intestine. *Science* **294**, 2155-2158,
1046 doi:10.1126/science.1065718 (2001).

1047 64 Dusing, M. R. & Wiginton, D. A. Epithelial lineages of the small intestine have unique
1048 patterns of GATA expression. *J Mol Histol* **36**, 15-24, doi:10.1007/s10735-004-2908-9
1049 (2005).

1050 65 Haveri, H. *et al.* Transcription factors GATA-4 and GATA-6 in normal and neoplastic
1051 human gastrointestinal mucosa. *BMC Gastroenterol* **8**, 9, doi:10.1186/1471-230X-8-9
1052 (2008).

1053 66 Netherland, C. & Thewke, D. P. Rimonabant is a dual inhibitor of acyl CoA:cholesterol
1054 acyltransferases 1 and 2. *Biochem Biophys Res Commun* **398**, 671-676,
1055 doi:10.1016/j.bbrc.2010.06.134 (2010).

1056 67 Ferraz-de-Souza, B. *et al.* Sterol O-acyltransferase 1 (SOAT1, ACAT) is a novel target of
1057 steroidogenic factor-1 (SF-1, NR5A1, Ad4BP) in the human adrenal. *J Clin Endocrinol*
1058 *Metab* **96**, E663-668, doi:10.1210/jc.2010-2021 (2011).

1059 68 Lewis, S. K. *et al.* DNA Methylation Analysis Validates Organoids as a Viable Model for
1060 Studying Human Intestinal Aging. *Cell Mol Gastroenterol Hepatol* **9**, 527-541,
1061 doi:10.1016/j.jcmgh.2019.11.013 (2020).

1062 69 Kasendra, M. *et al.* Development of a primary human Small Intestine-on-a-Chip using
1063 biopsy-derived organoids. *Sci Rep* **8**, 2871, doi:10.1038/s41598-018-21201-7 (2018).

1064 70 Dekkers, J. F. *et al.* High-resolution 3D imaging of fixed and cleared organoids. *Nat Protoc*
1065 **14**, 1756-1771, doi:10.1038/s41596-019-0160-8 (2019).

1066 71 Schindelin, J. *et al.* Fiji: an open-source platform for biological-image analysis. *Nat*
1067 *Methods* **9**, 676-682, doi:10.1038/nmeth.2019 (2012).

1068 72 Borten, M. A., Bajikar, S. S., Sasaki, N., Clevers, H. & Janes, K. A. Automated brightfield
1069 morphometry of 3D organoid populations by OrganoSeg. *Sci Rep* **8**, 5319,
1070 doi:10.1038/s41598-017-18815-8 (2018).

1071 73 Hafemeister, C. & Satija, R. Normalization and variance stabilization of single-cell RNA-
1072 seq data using regularized negative binomial regression. *Genome Biol* **20**, 296,
1073 doi:10.1186/s13059-019-1874-1 (2019).

1074 74 Miyoshi, H., Ajima, R., Luo, C. T., Yamaguchi, T. P. & Stappenbeck, T. S. Wnt5a
1075 potentiates TGF-beta signaling to promote colonic crypt regeneration after tissue injury.
1076 *Science* **338**, 108-113, doi:10.1126/science.1223821 (2012).

1077 75 Ootani, A. *et al.* Sustained in vitro intestinal epithelial culture within a Wnt-dependent stem
1078 cell niche. *Nat Med* **15**, 701-706, doi:10.1038/nm.1951 (2009).
1079

1080

Figure 1

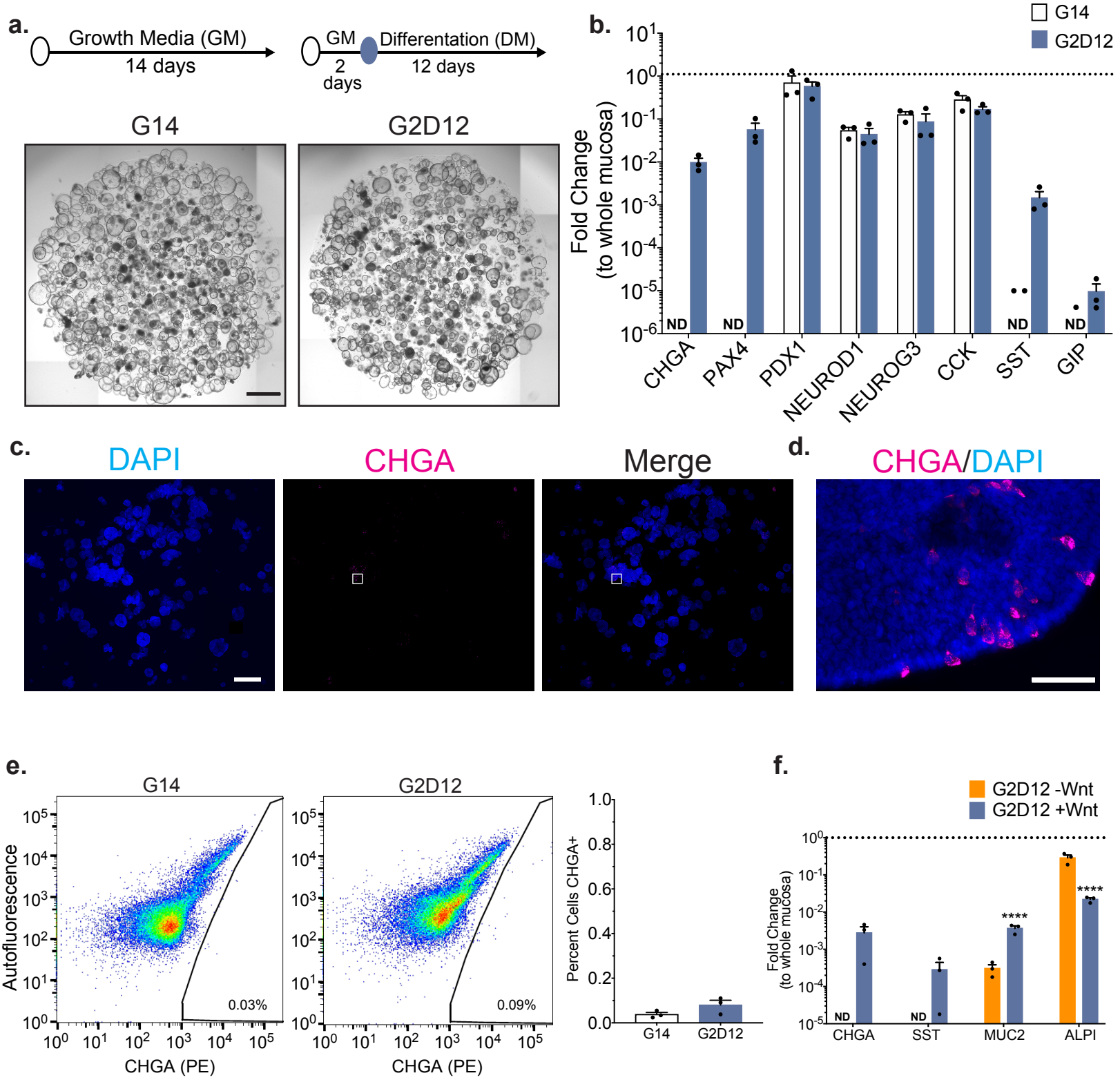
a.
Growth Media (GM)
14 days
GM
2 days
Differentation (DM)
12 days
G14
G2D12
b.
G14
G2D12
Fold Change (to whole mucosa)
ND
CHGA
PAX4
PDX1
NEUROD1
NEUROG3
CCK
SST
GIP
c.
DAPI
CHGA
Merge
d.
CHGA/DAPI
e.
G14
G2D12
Autofluorescence
CHGA (PE)
0.03%
0.09%
Percent Cells CHGA+
f.
G2D12 -Wnt
G2D12 +Wnt
Fold Change (to whole mucosa)
ND
****
CHGA
SST
MUC2
ALPI

1081 **FIGURE LEGENDS**

1082 **Figure 1. Base Differentiation Media Induces CHGA Expression in a Wnt-dependent**
1083 **Manner**

1084 (a) Representative light microscopy of enteroids (whole well) grown in growth media (GM) for 14
1085 days (G14) or two days in GM followed by 12 days in differentiation media (DM, G2D12).
1086 Specific culture schematic located above each panel, respectively. Scale bar = 1 mm.
1087 (b) qPCR analysis of enteroendocrine (EE) markers of enteroids grown in either G14 or G2D12
1088 compared to duodenal whole mucosa and normalized to *18S*. Dotted line denotes expression
1089 level in whole duodenal mucosa. Representative experiment showing n = 3 wells for each
1090 condition from a single enteroid line. *CHGA* = chromogranin A, *PAX4* = paired box 4, *PDX1* =
1091 pancreatic and duodenal homeobox 1, *NEUROD1* = neuronal differentiation 1, *NEUROG3* =
1092 neurogenin 3, *CCK* = cholecystokinin, *SST* = somatostatin, *GIP* = glucose-dependent
1093 insulinotropic peptide, ND = not detectable in 1 or more samples.
1094 (c and d) Representative immunofluorescence staining of CHGA (magenta) in enteroids (whole
1095 well) treated with G2D12. Boxed portion in (c) shown magnified in (d). DNA (4′,6-diamidino-2-
1096 phenylindole (DAPI) blue). Scale bars = 1 mm (c) and 50 μm (d).
1097 (e) Left two panels: Representative flow cytometry plots of CHGA-positive (CHGA+) cells from
1098 enteroids grown in either G14 or G2D12. Right panel: Percentage of CHGA+ cells per well.
1099 Representative experiment showing n = 3 wells from each condition from single enteroid line.
1100 (f) qPCR analysis of EE gene markers of enteroids grown in either G2D12 without Wnt (G2D12-
1101 Wnt) or with Wnt (G2D12+Wnt) compared to whole mucosa and normalized to *18S*. Dotted line
1102 denotes expression level in whole duodenal mucosa. *MUC2* = Mucin 2, *ALPI* = Intestinal
1103 alkaline phosphatase. Representative experiment showing n = 3 wells from each condition from
1104 a single enteroid line.
1105 Bars show mean ± SEM; two-way ANOVA with Tukey correction for multiple comparisons (**b**,**f**);
1106 two-tailed unpaired *t* test (**e**). ****$p < 0.0001$. Each experiment repeated with at least three

1107 different enteroid lines. Specific conditions were excluded from statistical analysis if the data
1108 from 1 or more samples was labeled as not detectable.
1109
1110
1111
1112
1113
1114
1115
1116
1117
1118
1119
1120
1121
1122
1123
1124
1125
1126
1127
1128
1129
1130
1131

Figure 2

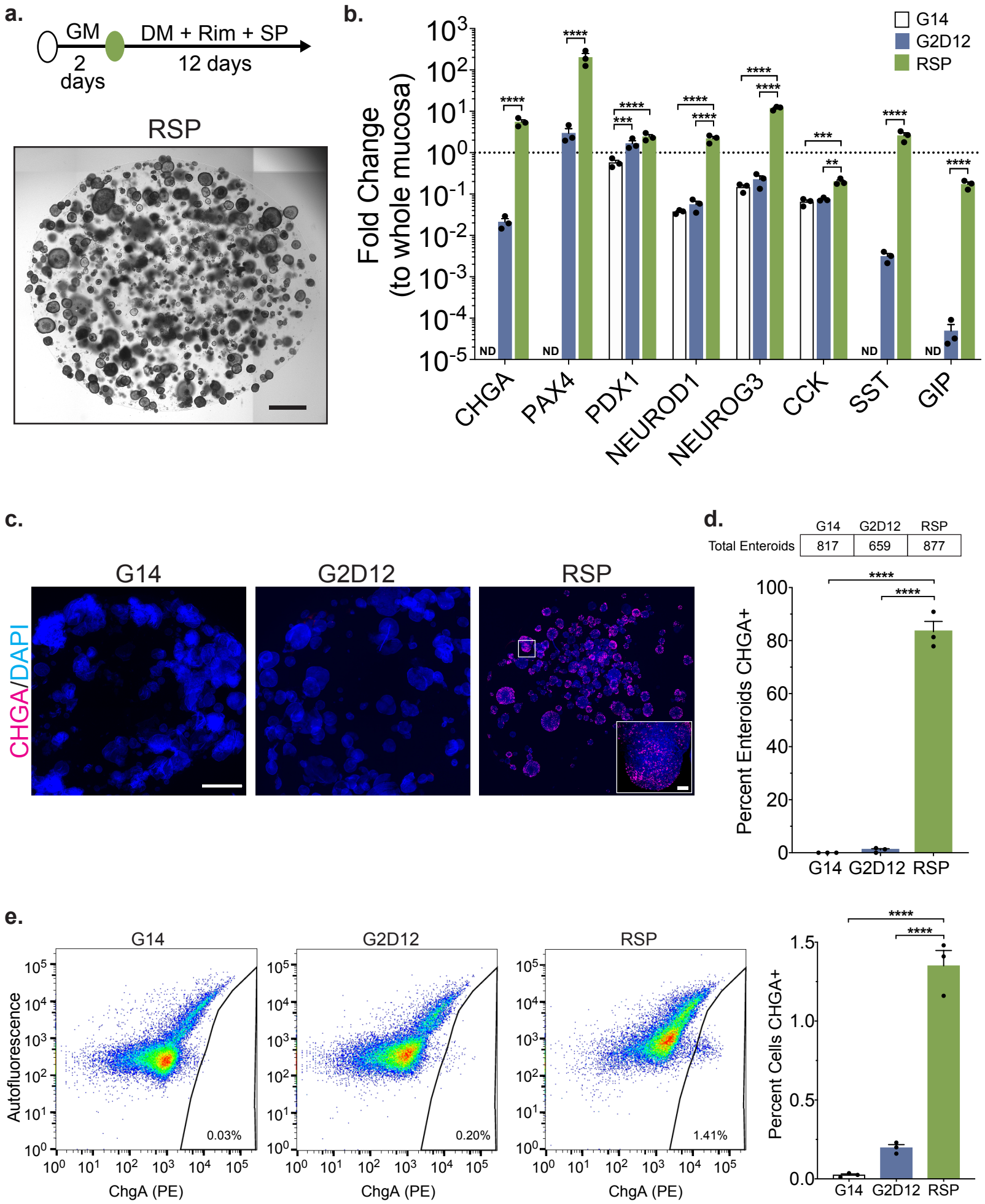
a.
GM
2 days
DM + Rim + SP
12 days
RSP
b.
G14
G2D12
RSP
Fold Change (to whole mucosa)
ND
CHGA
PAX4
PDX1
NEUROD1
NEUROG3
CCK
SST
GIP
c.
G14
G2D12
RSP
CHGA/DAPI
d.
Total Enteroids
G14 817
G2D12 659
RSP 877
Percent Enteroids CHGA+
e.
Autofluorescence
ChgA (PE)
0.03%
0.20%
1.41%
Percent Cells CHGA+

1132 **Figure 2. Differentiation with Small Molecules Rimonabant and SP600125 Induces CHGA**
1133 **Expression**

1134 (a) Representative light microscopy of enteroids (whole well) grown in growth media for two
1135 days followed by 12 days in differentiation media with rimonabant and SP600125 (RSP). Culture
1136 schematic located above panel. Scale bar = 1 mm.

1137 (b) qPCR analysis of enteroendocrine markers of enteroids grown in G14, G2D12 or RSP
1138 compared to duodenal whole mucosa and normalized to *18S*. Dotted line denotes expression
1139 level in whole duodenal mucosa. Representative experiment showing n = 3 wells from each
1140 condition from a single enteroid line. *CHGA* = chromogranin A, *PAX4* = paired box 4, *PDX1* =
1141 pancreatic and duodenal homeobox 1, *NEUROD1* = neuronal differentiation 1, *NEUROG3* =
1142 neurogenin 3, *CCK* = cholecystokinin, *SST* = somatostatin, *GIP* = glucose-dependent
1143 insulinotropic peptide, ND = not detectable in 1 or more samples.

1144 (c) Representative immunofluorescence staining of CHGA (magenta) in enteroids (whole well)
1145 treated with G14, G2D12 and RSP. Boxed portion magnified in lower right corner. Nuclei (4′,6-
1146 diamidino-2-phenylindole (DAPI), blue). Scale bars = 1mm and 50μm (boxed portion).

1147 (d) Percentage of enteroids with positive CHGA staining in G14, G2D12 and RSP treatments.
1148 Table above graph shows the total number of enteroids examined per condition. Average
1149 results are from three separate experiments from three different enteroid lines or passages.

1150 (e) Left three panels: Representative flow cytometry plots of CHGA+ cells from enteroids grown
1151 in G14, G2D12 or RSP. Right panel: Percentage of CHGA+ cells per well. Representative
1152 experiment showing n = 3 wells from each condition from a single enteroid line.

1153 Bars show mean ± SEM; two-way ANOVA with Tukey correction for multiple comparisons (**b**);
1154 one-way ANOVA with Tukey correction for multiple comparisons (**d**,**e**). **$p < 0.01$, ***$p < 0.001$,
1155 ****$p < 0.0001$. Each experiment repeated with at least three different enteroid lines. Specific
1156 conditions were excluded from statistical analysis if the data from 1 or more samples was
1157 labeled as not detectable.

Figure 3

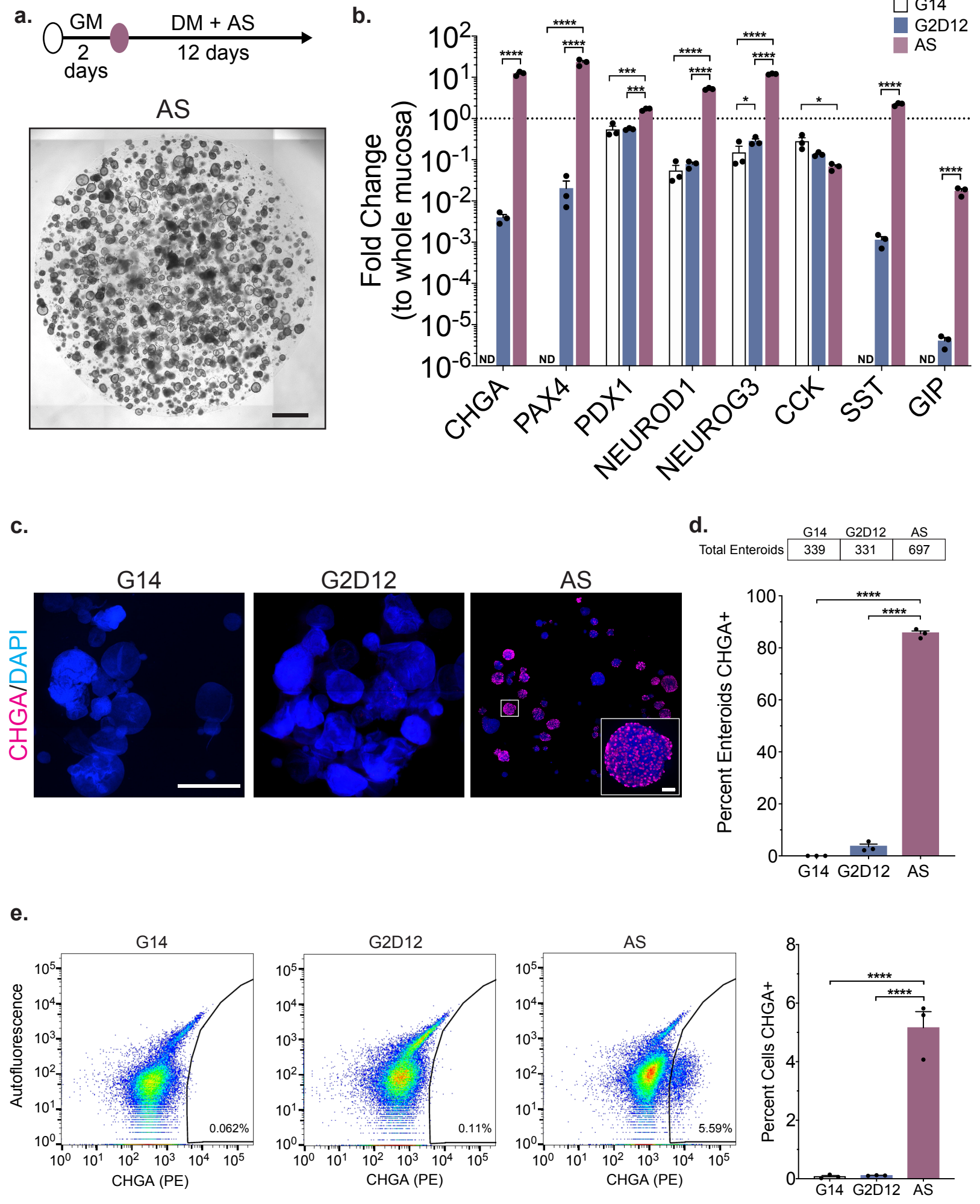
a.
GM
2 days
DM + AS
12 days
AS
b.
G14
G2D12
AS
Fold Change (to whole mucosa)
ND
CHGA
PAX4
PDX1
NEUROD1
NEUROG3
CCK
SST
GIP
c.
G14
G2D12
AS
CHGA/DAPI
d.
Total Enteroids
G14 339
G2D12 331
AS 697
Percent Enteroids CHGA+
e.
G14
G2D12
AS
Autofluorescence
CHGA (PE)
0.062%
0.11%
5.59%
Percent Cells CHGA+

1158 **Figure 3. Differentiation with Small Molecule AS1842856 Induces CHGA Expression**

1159 (a) Representative light microscopy of enteroids (whole well) grown in growth media for two
1160 days followed by 12 days in differentiation media with AS1842856 (AS). Culture schematic
1161 located above panel. Scale bar = 1 mm.

1162 (b) qPCR analysis of enteroendocrine markers of enteroids grown in G14, G2D12 or AS
1163 compared to whole duodenal mucosa and normalized to *18S*. Dotted line denotes expression
1164 level in whole duodenal mucosa. Representative experiment showing n = 3 wells from each
1165 condition from a single enteroid line. *CHGA* = chromogranin A, *PAX4* = paired box 4, *PDX1* =
1166 pancreatic and duodenal homeobox 1, *NEUROD1* = neuronal differentiation 1, *NEUROG3* =
1167 neurogenin 3, *CCK* = cholecystokinin, *SST* = somatostatin, *GIP* = glucose-dependent
1168 insulinotropic peptide, ND = not detectable in 1 or more samples.

1169 (c) Representative immunofluorescence staining of CHGA (magenta) in enteroids (whole well)
1170 treated with G14, G2D12 and AS. Boxed portion magnified in lower right corner. DNA (4′,6-
1171 diamidino-2-phenylindole (DAPI), blue). Scale bars = 1 mm and 50 μm (boxed portion).

1172 (d) Percentage of enteroids with positive CHGA staining in G14, G2D12 and AS treatments.
1173 Table above graph shows the total number of enteroids examined per condition. Average
1174 results are from three separate experiments from three different enteroid lines or passages.

1175 (e) Left three panels: Representative flow cytometry plots of CHGA+ cells from enteroids grown
1176 in G14, G2D12 or AS. Right panel: Percentage of CHGA+ cells per well. Representative
1177 experiment showing n = 3 wells from each condition from a single enteroid line.

1178 Bars show mean ± SEM; two-way ANOVA with Tukey correction for multiple comparisons (**b**);
1179 one-way ANOVA with Tukey correction for multiple comparisons (**d**,**e**). *$p < 0.05$, ***$p < 0.001$,
1180 ****$p < 0.0001$. Each experiment repeated with at least three different enteroid lines. Specific
1181 conditions were excluded from statistical analysis if the data from 1 or more samples was
1182 labeled as not detectable.

1183

Figure 4

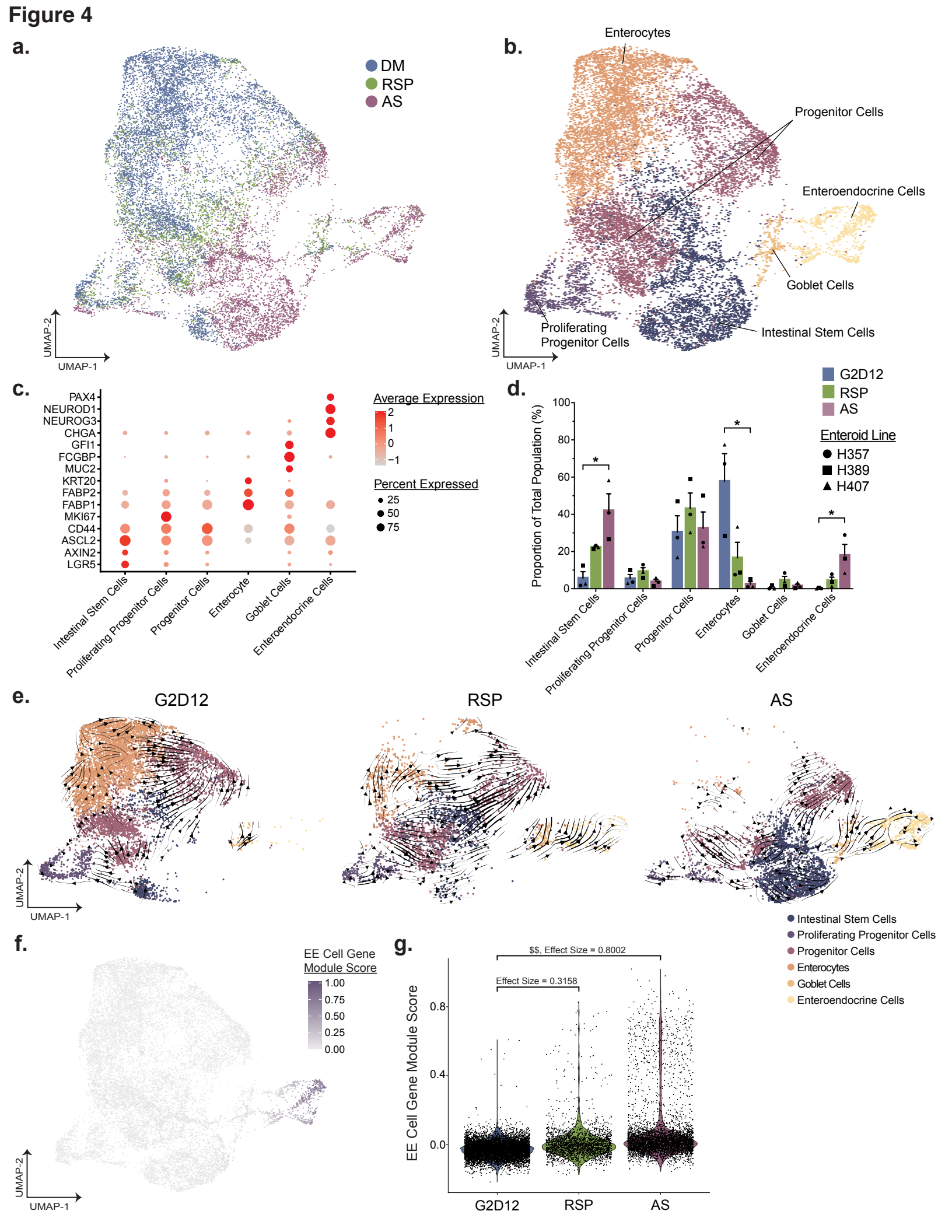
a.
DM
RSP
AS
UMAP-2
UMAP-1
b.
Enterocytes
Progenitor Cells
Enteroendocrine Cells
Goblet Cells
Proliferating Progenitor Cells
Intestinal Stem Cells
UMAP-2
UMAP-1
c.
PAX4
NEUROD1
NEUROG3
CHGA
GFI1
FCGBP
MUC2
KRT20
FABP2
FABP1
MKI67
CD44
ASCL2
AXIN2
LGR5
Intestinal Stem Cells
Proliferating Progenitor Cells
Progenitor Cells
Enterocyte
Goblet Cells
Enteroendocrine Cells
Average Expression
2
1
0
−1
Percent Expressed
25
50
75
d.
G2D12
RSP
AS
Enteroid Line
H357
H389
H407
Proportion of Total Population (%)
100
80
60
40
20
0
*
*
*
Intestinal Stem Cells
Proliferating Progenitor Cells
Progenitor Cells
Enterocytes
Goblet Cells
Enteroendocrine Cells
e.
G2D12
RSP
AS
UMAP-2
UMAP-1
Intestinal Stem Cells
Proliferating Progenitor Cells
Progenitor Cells
Enterocytes
Goblet Cells
Enteroendocrine Cells
f.
EE Cell Gene
Module Score
1.00
0.75
0.50
0.25
0.00
UMAP-2
UMAP-1
g.
$$, Effect Size = 0.8002
Effect Size = 0.3158
EE Cell Gene Module Score
0.8
0.4
0.0
G2D12
RSP
AS

1184 **Figure 4. scRNA-seq Profiling of Enteroids Cultured with Rimonabant/SP600125 or**
1185 **AS1842856**
1186 (a) Uniform manifold approximation and projection (UMAP) visualization of 14,767 cells
1187 summarizing enteroid differentiation from all samples, color labeled by culture condition.
1188 (b) UMAP visualization from (a), color labeled by broad annotated cell identity, following Louvain
1189 clustering.
1190 (c) Dot plot of the average scaled expression (measured by average Pearson residual) of
1191 canonical markers of various gut epithelial cell types, plotted against cluster identity.
1192 (d) Proportional abundance of epithelial cell subsets by enteroid culture protocol. Each culture
1193 condition consists of three different enteroid lines from distinct human donors, as denoted by
1194 data point shape. Bars show mean ± SEM; Kruskal-Wallis test with Dunn's post-hoc analysis
1195 displayed. P values were adjusted using Bonferroni correction for multiple comparisons. *p
1196 <0.05.
1197 (e) UMAP visualization of 14,767 cells divided by culture condition and colored by cell identity.
1198 Trajectory analysis of each protocol was calculated using scVelo and the vector field was
1199 overlaid on top of each UMAP. Arrows represent smoothed averages of the estimated cellular
1200 differentiation trajectory, with arrow thickness corresponding to the "speed" of differentiation.
1201 (f) UMAP visualization from (a), with individual cells colored by their EE cell module score. Each
1202 score was scaled on a range from 0 to 1.
1203 (g) Violin plots of the module score described in (f) split across culture condition. The effect size
1204 between culture conditions was calculated as Cohen's d; $$ 0.8 < d < 1.2.
1205
1206
1207
1208

Figure 5

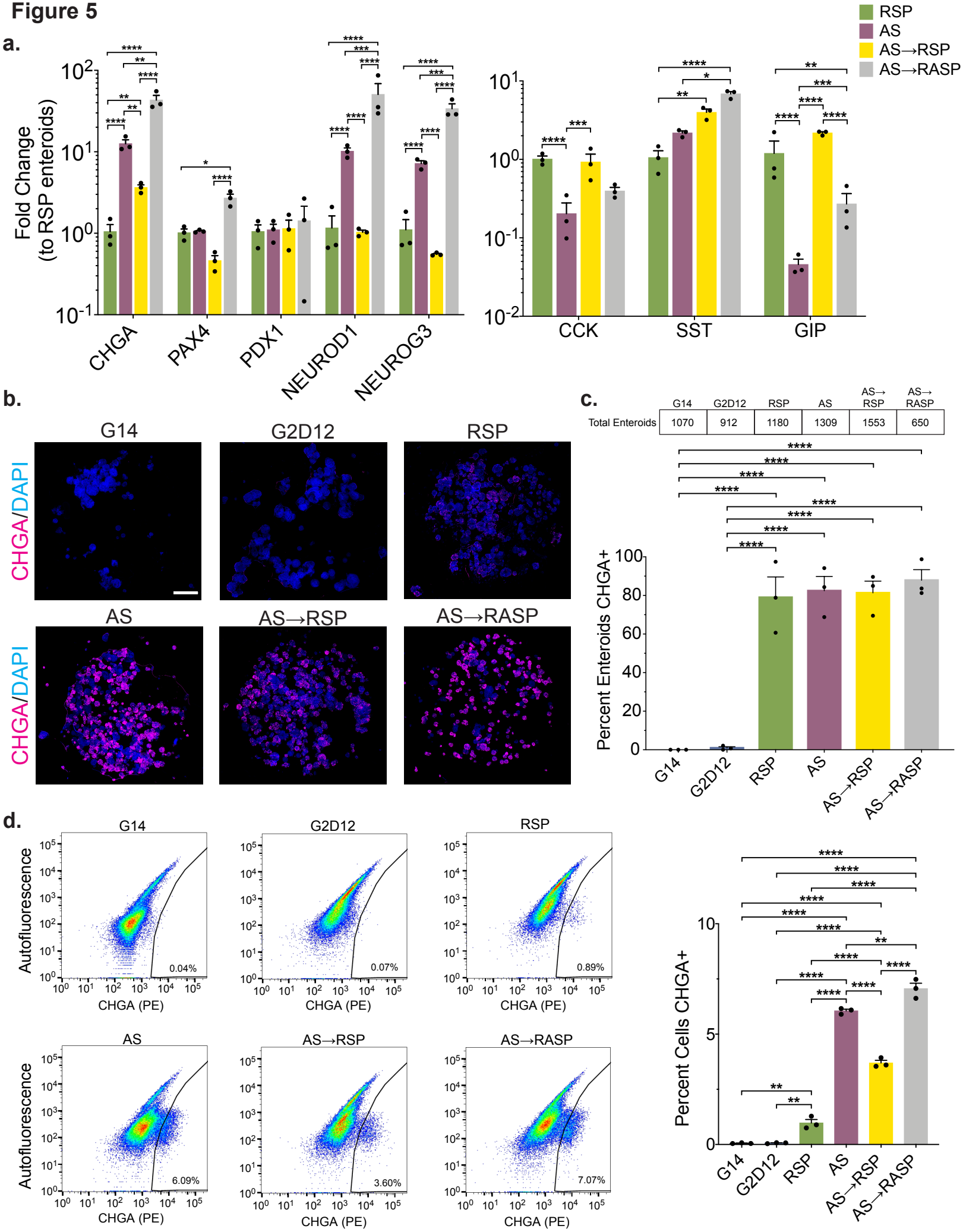
a.
RSP
AS
AS→RSP
AS→RASP
Fold Change (to RSP enteroids)
CHGA
PAX4
PDX1
NEUROD1
NEUROG3
CCK
SST
GIP
b.
G14
G2D12
RSP
AS
AS→RSP
AS→RASP
CHGA/DAPI
c.
Total Enteroids
G14 1070
G2D12 912
RSP 1180
AS 1309
AS→RSP 1553
AS→RASP 650
Percent Enteroids CHGA+
d.
Autofluorescence
CHGA (PE)
0.04%
0.07%
0.89%
6.09%
3.60%
7.07%
Percent Cells CHGA+

1209 **Figure 5. Combinations of AS1842856 and Rimonabant/SP600125 Induce Different Levels**
1210 **of Enteroendocrine Marker Expression**

1211 (a) qPCR analysis of enteroendocrine markers of enteroids grown in AS, AS for 6 days, followed
1212 by RSP only for 6 days (AS→RSP) and AS for 6 days, followed by AS and RSP for 6 days
1213 (AS→RASP) compared to enteroids grown in RSP and normalized to *18S*. Representative
1214 experiment showing n = 3 wells from each condition from a single enteroid line. *CHGA* =
1215 chromogranin A, *PAX4* = paired box 4, *PDX1* = pancreatic and duodenal homeobox 1,
1216 *NEUROD1* = neuronal differentiation 1, *NEUROG3* = neurogenin 3, *CCK* = cholecystokinin,
1217 *SST* = somatostatin, *GIP* = glucose-dependent insulinotropic peptide.

1218 (b) Representative immunofluorescence staining of CHGA (magenta) in enteroids (whole well)
1219 treated with G14, G2D12, RSP, AS, AS→RSP, and AS→RASP. DNA (4′,6-diamidino-2-
1220 phenylindole (DAPI), blue). Scale bar = 1 mm.

1221 (c) Percentage of enteroids with positive CHGA staining in G14, G2D12, AS, RSP, AS→RSP,
1222 and AS→RASP treatments. Table above graph shows the total number of enteroids examined
1223 per condition. Average results are from three separate experiments from three different enteroid
1224 lines or passages.

1225 (d) Left six panels: Representative flow cytometry plots of CHGA+ cells from enteroids grown in
1226 G14, G2D12, RSP, AS, AS to RSP, and AS to RASP. Right panel: Percentage of CHGA+ cells
1227 per well. Representative experiment showing n = 3 wells from each condition from a single
1228 enteroid line.

1229 Bars show mean ± SEM; two-way ANOVA with Tukey correction for multiple comparisons (**a**);
1230 one-way ANOVA with Tukey correction for multiple comparisons (**c**,**d**). *p <0.05, **p < 0.01, ***p
1231 < 0.001, ****p < 0.0001. Each experiment repeated with at least three different enteroid lines.

1232

1233

Figure 6

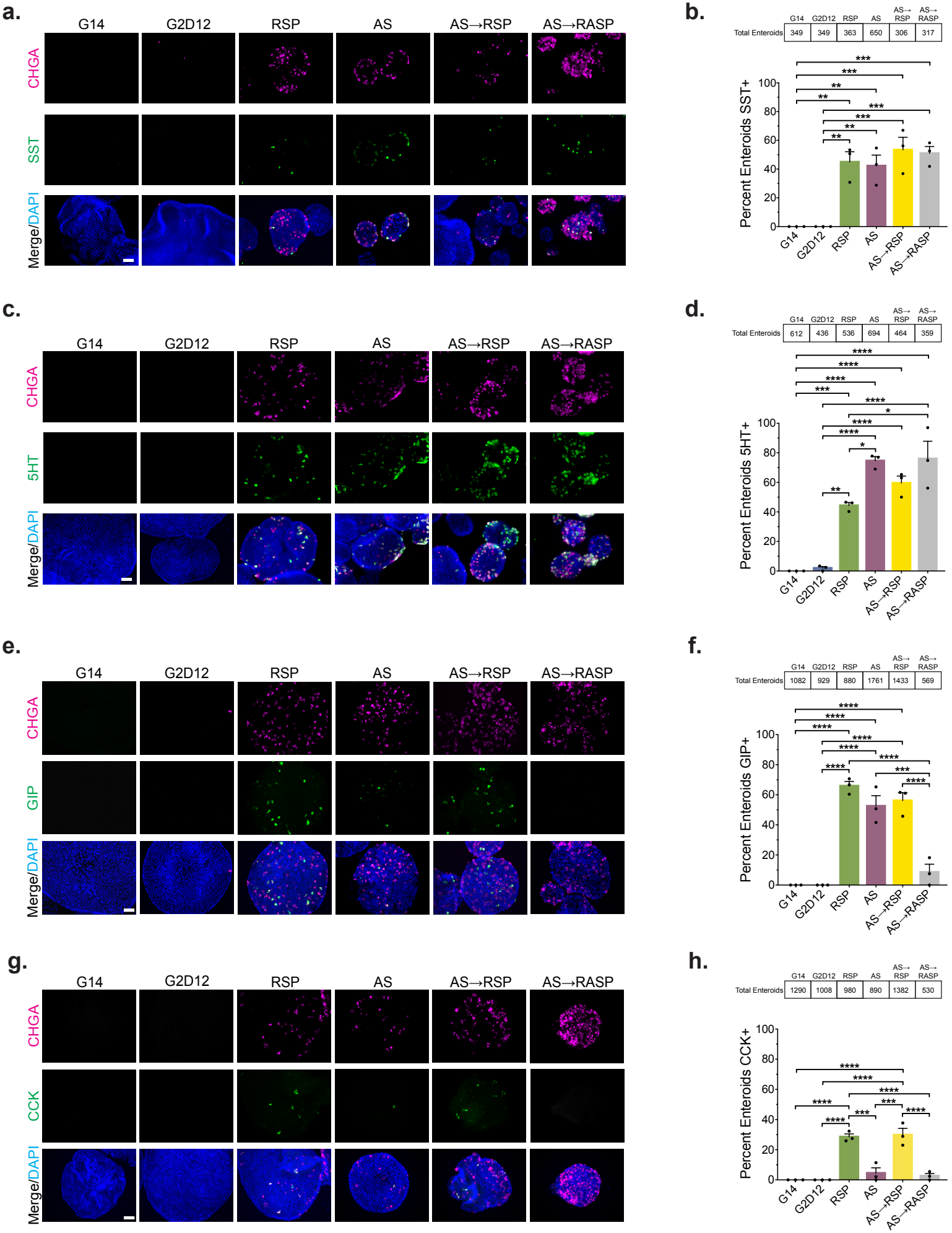
a.
G14
G2D12
RSP
AS
AS→RSP
AS→RASP
CHGA
SST
Merge/DAPI
b.
Total Enteroids 349 349 363 650 306 317
Percent Enteroids SST+
c.
CHGA
5HT
Merge/DAPI
d.
Total Enteroids 612 436 536 694 464 359
Percent Enteroids 5HT+
e.
CHGA
GIP
Merge/DAPI
f.
Total Enteroids 1082 929 880 1761 1433 569
Percent Enteroids GIP+
g.
CHGA
CCK
Merge/DAPI
h.
Total Enteroids 1290 1008 980 890 1382 530
Percent Enteroids CCK+

1234 **Figure 6. Multiple Differentiation Conditions Induce Hormone Production**

1235 (a) Representative immunofluorescence staining of somatostatin (SST, green) and
1236 chromogranin A (CHGA, magenta) in enteroids treated with G14, G2D12, RSP, AS, AS→RSP,
1237 and AS→RASP. DNA (4′,6-diamidino-2-phenylindole (DAPI), blue). Scale bar = 50μm.

1238 (b) Percentage of enteroids with positive SST staining in G14, G2D12, RSP, AS, AS→RSP, and
1239 AS→RASP treatments. Tables above graphs show the total number of enteroids examined per
1240 condition. Average results are from three separate experiments from three different enteroid
1241 lines or passages. Each experiment repeated with at least three different enteroid lines.

1242 (c) Representative immunofluorescence staining of serotonin (5HT, green) and CHGA
1243 (magenta) in enteroids treated with G14, G2D12, RSP, AS, AS→RSP and AS→RASP. DNA
1244 (DAPI, blue). Scale bar = 50 μm.

1245 (d) Percentage of enteroids with positive 5HT staining in G14, G2D12, RSP, AS, AS→RSP and
1246 AS→RASP treatments. Tables above graphs show the total number of enteroids examined per
1247 condition. Average results are from three separate experiments from three different enteroid
1248 lines or passages. Each experiment repeated with at least three different enteroid lines.

1249 (e) Representative immunofluorescence staining of glucose-dependent insulinotropic peptide
1250 (GIP, green) and CHGA (magenta) in enteroids treated with G14, G2D12, RSP, AS, AS→RSP,
1251 and AS→RASP. DNA (DAPI, blue). Scale bar = 50 μm.

1252 (f) Percentage of enteroids with positive GIP staining in G14, G2D12, RSP, AS, AS→RSP, and
1253 AS→RASP treatments. Tables above graphs show the total number of enteroids examined per
1254 condition. Average results are from three separate experiments from three different enteroid
1255 lines or passages. Each experiment repeated with at least three different enteroid lines.

1256 (g) Representative immunofluorescence staining of cholecystokinin (CCK, green) and CHGA
1257 (magenta) in enteroids treated with G14, G2D12, RSP, AS, AS→RSP, and AS→RASP. DNA
1258 (DAPI, blue). Scale bar = 50 μm.

1259 (h) Percentage of enteroids with positive CCK staining in G14, G2D12, RSP, AS, AS→RSP,
1260 and AS→RASP treatments. Tables above graphs show the total number of enteroids examined
1261 per condition. Average results are from three separate experiments from three different enteroid
1262 lines or passages. Each experiment repeated with at least three different enteroid lines.
1263 Bars show mean ± SEM; one-way ANOVA with Tukey correction for multiple comparisons
1264 (**b**,**d**,**f**,**h**). *$p < 0.05$, **$p < 0.01$, ***$p < 0.001$, ****$p < 0.0001$.
1265
1266
1267
1268
1269
1270
1271
1272
1273
1274
1275
1276
1277
1278
1279
1280
1281
1282
1283

Figure 7

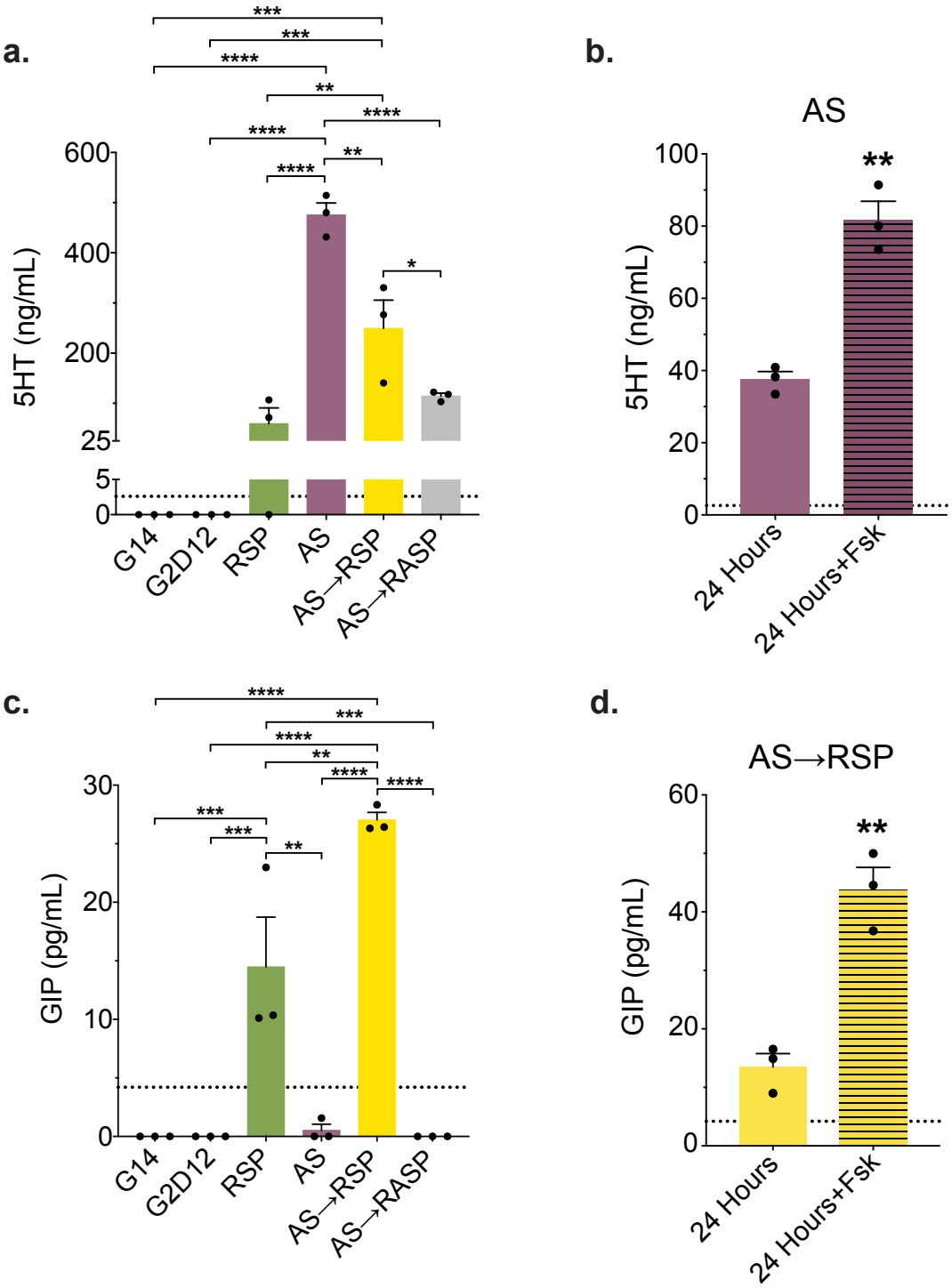
a.
5HT (ng/mL)
600
400
200
25
5
0
***
***
****
**
****
****
****
**
*
G14
G2D12
RSP
AS
AS→RSP
AS→RASP
b.
AS
5HT (ng/mL)
100
80
60
40
20
0
**
24 Hours
24 Hours+Fsk
c.
GIP (pg/mL)
30
20
10
0
****
***
****
**
****
****
***
***
**
G14
G2D12
RSP
AS
AS→RSP
AS→RASP
d.
AS→RSP
GIP (pg/mL)
60
40
20
0
**
24 Hours
24 Hours+Fsk

1284 **Figure 7. Differentiation Conditions Induce Hormone Secretion**

1285 (a) Serotonin (5HT) ELISA of conditioned media from the last two days of differentiation of
1286 enteroids grown in G14, G2D12, RSP, AS, AS→RSP, and AS→RASP. Dotted line at 2.6 ng/mL
1287 represents the lower limit of detection for the assay. Representative experiment showing n = 3
1288 wells from each condition from a single enteroid line.

1289 (b) 5HT ELISA of AS conditioned media collected after 24 hours on day 13 (solid bar) and after
1290 24 hours with forskolin (Fsk) on day 14 (striped bar). Dotted line at 2.6 ng/mL represents the
1291 lower limit of detection for the assay. Representative experiment showing n = 3 wells from each
1292 condition from a single enteroid line.

1293 (c) Glucose-dependent insulinotropic peptide (GIP) ELISA of conditioned media from the last
1294 two days of differentiation of enteroids grown in G14, G2D12, RSP, AS, AS→RSP, and
1295 AS→RASP. Dotted line at 4.2 pg/mL represents the lower limit of detection for the assay.
1296 Representative experiment showing n = 3 wells from each condition from a single enteroid line.

1297 (d) GIP ELISA of AS→RSP conditioned media collected after 24 hours on day 13 (solid bar) and
1298 after 24 hours with Fsk on day 14 (striped bar). Dotted line at 4.2 pg/mL represents the lower
1299 limit of detection for the assay. Representative experiment showing n = 3 wells from each
1300 condition from a single enteroid line.

1301 Bars show mean ± SEM; one-way ANOVA with Tukey correction for multiple comparisons (**a**,**c**);
1302 two-tailed unpaired *t* test (**b**,**d**). *$p < 0.05$, **$p < 0.01$, ***$p < 0.001$, ****$p < 0.0001$. Each
1303 experiment repeated with at least three different enteroid lines.

1304

1305

1306

1307

1308

Figure 8

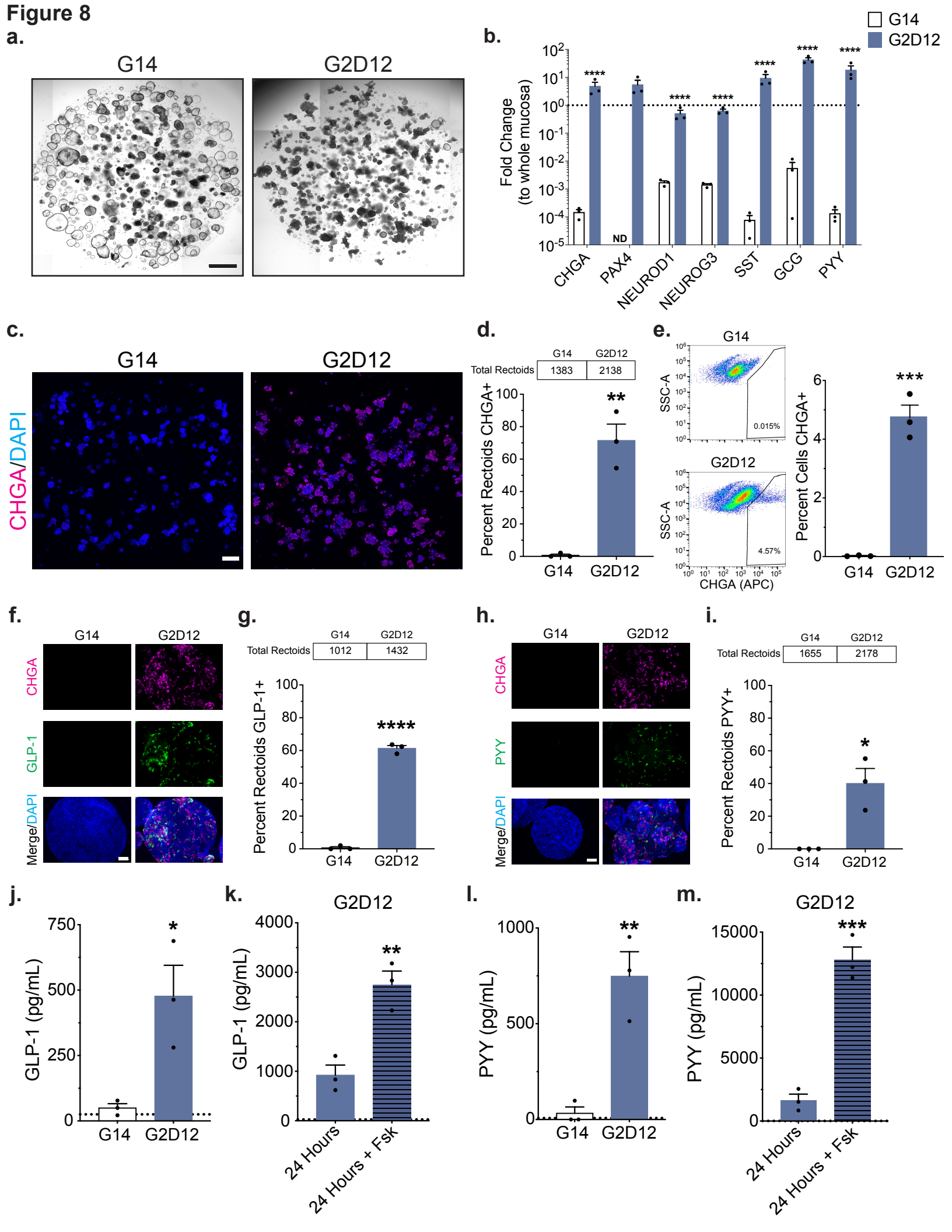
a.
G14
G2D12
b.
G14
G2D12
Fold Change (to whole mucosa)
ND
CHGA
PAX4
NEUROD1
NEUROG3
SST
GCG
PYY
c.
G14
G2D12
CHGA/DAPI
d.
Total Rectoids
G14 1383
G2D12 2138
Percent Rectoids CHGA+
e.
G14
G2D12
SSC-A
CHGA (APC)
0.015%
4.57%
Percent Cells CHGA+
f.
G14
G2D12
CHGA
GLP-1
Merge/DAPI
g.
Total Rectoids
G14 1012
G2D12 1432
Percent Rectoids GLP-1+
h.
G14
G2D12
CHGA
PYY
Merge/DAPI
i.
Total Rectoids
G14 1655
G2D12 2178
Percent Rectoids PYY+
j.
GLP-1 (pg/mL)
G14
G2D12
k.
G2D12
GLP-1 (pg/mL)
24 Hours
24 Hours + Fsk
l.
PYY (pg/mL)
G14
G2D12
m.
G2D12
PYY (pg/mL)
24 Hours
24 Hours + Fsk

1309 **Figure 8. Induction of the Enteroendocrine Lineage in Rectoids**

1310 (a) Representative light microscopy of rectoids (whole well) grown in growth media for 14 days
1311 (G14) or two days in GM followed by 12 days in differentiation media (G2D12). Scale bar = 1
1312 mm.

1313 (b) qPCR analysis of enteroendocrine (EE) markers of rectoids grown in either G14 or G2D12
1314 compared to whole rectal mucosa and normalized to *18S*. Dotted line denotes expression level
1315 in whole rectal mucosa. Representative experiment showing n = 3 wells for each condition from
1316 a single enteroid line. *CHGA* = chromogranin A, *PAX4* = paired box 4, *NEUROD1* = neuronal
1317 differentiation 1, *NEUROG3* = neurogenin 3, *SST* = somatostatin, *GCG* = glucagon, *PYY* =
1318 peptide YY, ND = not detectable in 1 or more samples.

1319 (c) Representative immunofluorescence staining of CHGA (magenta) in rectoids (whole well)
1320 treated with G14 and G2D12. DNA (4′,6-diamidino-2-phenylindole (DAPI), blue). Scale bar = 1
1321 mm.

1322 (d) Percentage of rectoids with positive CHGA staining in G14 and G2D12 treatments. Table
1323 above graph shows the total number of rectoids examined per condition. Average results are
1324 from three separate experiments from three different enteroid lines or passages.

1325 (e) Left two panels: Representative flow cytometry plots of CHGA+ cells from rectoids grown in
1326 G14 and G2D12. Right panel: Percentage of CHGA+ cells per well. Representative experiment
1327 showing n = 3 wells from each condition from a single enteroid line.

1328 (f) Representative immunofluorescence staining of glucagon-like peptide-1 (GLP-1, green) and
1329 CHGA (magenta) in rectoids treated with G14 and G2D12. DNA (DAPI, blue). Scale bar = 50
1330 μm.

1331 (g) Percentage of rectoids with positive GLP-1 staining in G14 and G2D12. Table above graph
1332 show the total number of rectoids examined per condition. Average results are from three
1333 separate experiments from three different enteroid lines or passages.

1334 (h) Representative immunofluorescence staining of peptide YY (PYY, green) and CHGA
1335 (magenta) in rectoids treated with G14 and G2D12. DNA (DAPI, blue). Scale bar = 50 μm.
1336 (i) Percentage of rectoids with positive PYY staining in G14 and G2D12. Table above graph
1337 show the total number of rectoids examined per condition. Average results are from three
1338 separate experiments from three different enteroid lines or passages.
1339 (j) GLP-1 ELISA of conditioned media from the last two days of differentiation of rectoids grown
1340 in G14 and G2D12. Dotted line at 25 pg/mL represents the lower limit of detection for the assay.
1341 Representative experiment showing n = 3 wells from each condition from a single rectoid line.
1342 (k) GLP-1 ELISA of G2D12 conditioned media collected after 24 hours on day 13 (solid bar) and
1343 after 24 hours with forskolin (Fsk) on day 14 (striped bar). Dotted line at 25 pg/mL represents
1344 the lower limit of detection for the assay. Representative experiment showing n = 3 wells from
1345 each condition from a single rectoid line.
1346 (l) PYY ELISA of conditioned media from the last two days of differentiation of rectoids grown in
1347 G14 and G2D12. Dotted line at 7.3 pg/mL represents the lower limit of detection for the assay.
1348 Representative experiment showing n = 3 wells from each condition from a single rectoid line.
1349 (m) PYY ELISA of G2D12 conditioned media collected after 24 hours on day 13 (solid bar) and
1350 after 24 hours with forskolin (Fsk) on day 14 (striped bar). Dotted line at 7.3 pg/mL represents
1351 the lower limit of detection for the assay. Representative experiment showing n = 3 wells from
1352 each condition from a single rectoid line.
1353 Bars show mean ± SEM; two-way ANOVA with Tukey correction for multiple comparisons (**b**);
1354 two-tailed unpaired *t* test (**d**,**e**,**g**,**i**,**j**,**k**,**l**,**m**). *$p < 0.05$, **$p < 0.01$, ***$p < 0.001$, ****$p < 0.0001$.
1355 Each experiment repeated with at least three different rectoid lines. Specific conditions were
1356 excluded from statistical analysis if the data from 1 or more samples was labeled as not
1357 detectable.
1358
1359